LETTER

doi:10.1038/nature22359

CPS1 maintains pyrimidine pools and DNA synthesis in KRAS/LKB1-mutant lung cancer cells

Jiyeon Kim[1], Zeping Hu[1], Ling Cai[1], Kailong Li[1], Eunhee Choi[2], Brandon Faubert[1], Divya Bezwada[1], Jaime Rodriguez-Canales[3], Pamela Villalobos[3], Yu-Fen Lin[4], Min Ni[1], Kenneth E. Huffman[5], Luc Girard[5], Lauren A. Byers[6], Keziban Unsal-Kacmaz[7], Christopher G. Peña[8]†, John V. Heymach[6], Els Wauters[9], Johan Vansteenkiste[9], Diego H. Castrillon[8], Benjamin P. C. Chen[4], Ignacio Wistuba[3], Diether Lambrechts[10,11], Jian Xu[1], John D. Minna[5] & Ralph J. DeBerardinis[1,12,13]

Metabolic reprogramming by oncogenic signals promotes cancer initiation and progression. The oncogene *KRAS* and tumour suppressor *STK11*, which encodes the kinase LKB1, regulate metabolism and are frequently mutated in non-small-cell lung cancer (NSCLC). Concurrent occurrence of oncogenic *KRAS* and loss of LKB1 (KL) in cells specifies aggressive oncological behaviour[1,2]. Here we show that human KL cells and tumours share metabolomic signatures of perturbed nitrogen handling. KL cells express the urea cycle enzyme carbamoyl phosphate synthetase-1 (CPS1), which produces carbamoyl phosphate in the mitochondria from ammonia and bicarbonate, initiating nitrogen disposal. Transcription of CPS1 is suppressed by LKB1 through AMPK, and CPS1 expression correlates inversely with LKB1 in human NSCLC. Silencing CPS1 in KL cells induces cell death and reduces tumour growth. Notably, cell death results from pyrimidine depletion rather than ammonia toxicity, as CPS1 enables an unconventional pathway of nitrogen flow from ammonia into pyrimidines. CPS1 loss reduces the pyrimidine to purine ratio, compromises S-phase progression and induces DNA-polymerase stalling and DNA damage. Exogenous pyrimidines reverse DNA damage and rescue growth. The data indicate that the KL oncological genotype imposes a metabolic vulnerability related to a dependence on a cross-compartmental pathway of pyrimidine metabolism in an aggressive subset of NSCLC.

Given that KL status influences metabolic vulnerabilities[3,4], we compared the metabolomes of NSCLC cells with mutant *KRAS* (K) to those with mutant *KRAS* plus LKB1 loss (KL) (Extended Data Fig. 2 and Supplementary Table 1). Supervised analysis revealed that most metabolites that were discriminatory between the two genotypes were involved in nitrogen metabolism (Fig. 1a, Supplementary Table 2 and Supplementary Discussion). Metabolomics of human NSCLC also revealed altered nitrogen metabolism in KL tumours (Extended Data Figs 2, 3 and Supplementary Tables 3, 4). Several urea cycle metabolites accumulated in KL cell lines, and mRNA expression of 203 human cell lines (144 lung cancer and 59 bronchial or small airway epithelial cell lines) showed that there is increased *CPS1* expression in KL cells (Fig. 1b, c, Extended Data Fig. 1c and Supplementary Tables 5, 6). CPS1 catalyses the rate-limiting step of the urea cycle (Fig. 1b). Genes encoding other urea cycle enzymes, and expression and activity of nitric oxide synthase, which connects metabolically with the urea cycle, were not markedly altered among genotypes (Extended Data Figs 1b, 4a–c).

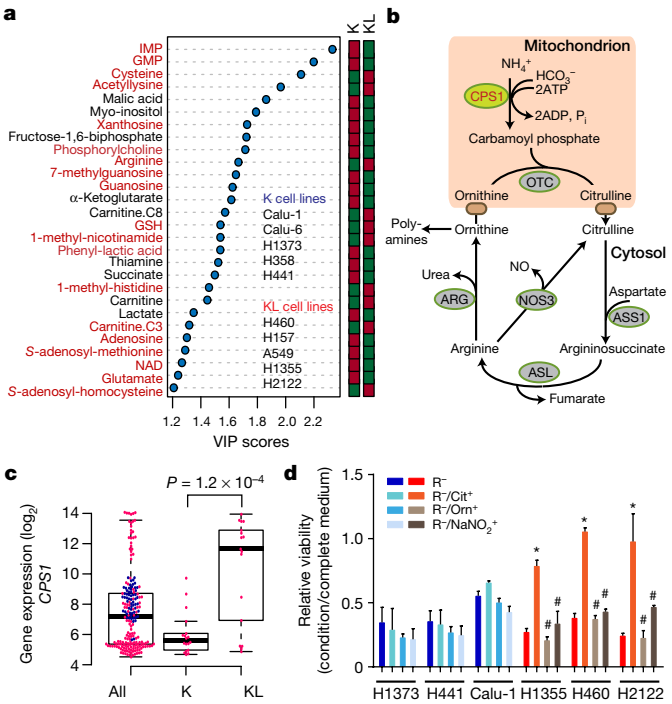

Figure 1 | Altered urea cycle metabolism in KL cells. a, Metabolites differentiating between five K and five KL cell lines. Shown as variable importance in the projection (VIP) score (VIP > 1.0, metabolites with VIP > 1.2 are shown). Metabolites from nitrogen-related pathways are in red. Relative metabolite abundance is indicated in the bar, with red representing metabolite accumulation. **b**, Schematic of the urea cycle. NO, nitric oxide. **c**, Distribution of *CPS1* mRNA abundance in 203 cell lines, including 18 K and 17 KL cell lines. Pink dots are cancer cell lines and blue dots are bronchial or small airway epithelial cell lines. **d**, Sensitivity to arginine deprivation (R^-) with or without metabolite supplementation in selected K (blue) and KL (red or grey) cell lines. Cit, citrulline; $NaNO_2$, sodium nitrite; Orn, ornithine. Data are the mean ± s.d. of three independent cultures. Statistical significance was assessed using a two-tailed Student's *t*-test (**c**) or one-way ANOVA with Tukey's multiple comparisons test (**d**). In **d**, $*P < 0.05$ compared to R^-; $\#P < 0.05$ compared to R^-Cit^+. Metabolomics were performed once, and viability was measured twice.

[1]Children's Medical Center Research Institute, UT Southwestern Medical Center, Dallas, Texas 75390, USA. [2]Department of Pharmacology, UT Southwestern Medical Center, Dallas, Texas 75390, USA. [3]Department of Translational Molecular Pathology, University of Texas MD Anderson Cancer Center, 2130 West Holcombe Boulevard, Houston, Texas 77030, USA. [4]Department of Radiation Oncology, UT Southwestern Medical Center, Dallas, Texas 75390, USA. [5]Hamon Center for Therapeutic Oncology, UT Southwestern Medical Center, Dallas, Texas 75390, USA. [6]Department of Thoracic/Head and Neck Medical Oncology, University of Texas MD Anderson Cancer Center, 2130 West Holcombe Boulevard, Houston, Texas 77030, USA. [7]Oncology Research Unit, Pfizer, 401 North Middletown Road, Pearl River, New York 10965, USA. [8]Department of Pathology, UT Southwestern Medical Center, Dallas, Texas 75390, USA. [9]Respiratory Division, University of Gasthuisberg, KU Leuven, Herestraat 49, 3000 Leuven, Belgium. [10]Laboratory for Translational Genetics, Department of Human Genetics, KU Leuven, O&N 4 Herestraat 49 – box 912, 3000 Leuven, Belgium. [11]VIB Center for Cancer Biology, KU Leuven, O&N 4 Herestraat 49 – box 912, 3000 Leuven, Belgium. [12]Department of Pediatrics, UT Southwestern Medical Center, Dallas, Texas 75390, USA. [13]McDermott Center for Human Growth and Development, UT Southwestern Medical Center, Dallas, Texas 75390, USA. †Present address: University of Texas Health Science Center San Antonio, 7703 Floyd Curl Drive, San Antonio, Texas 78229, USA.

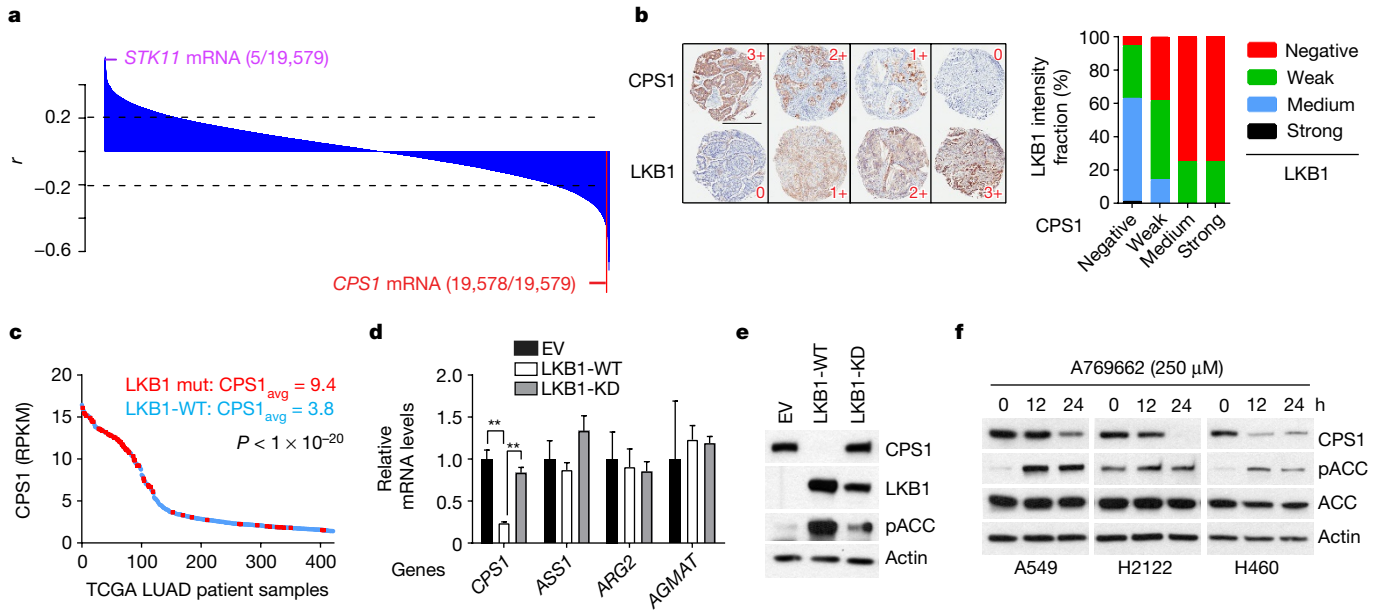

Figure 2 | LKB1 negatively regulates CPS1 transcription. a, Pearson's correlation coefficient (r) between LKB1 protein and 19,579 transcripts in 94 cell lines. Dashed lines demarcate $P = 0.05$. **b**, Left, representative tissue microarray (TMA) staining for CPS1 and LKB1, indicating negative (0), weak (1+), medium (2+) and strong (3+) staining. Scale bar, 600 μm. Right, LKB1 expression in each CPS1 expression group (total $n = 180$). **c**, *CPS1* mRNA abundance in human lung adenocarcinoma ($n = 483$). LKB1 mutants (mut) are shown in red. RPKM, reads per kilobase per million reads; WT, wild type. **d**, Urea cycle-related enzyme expression in control H460 cells (EV, empty vector, $n = 3$) and cells expressing wild-type ($n = 3$) or kinase-dead (KD; K78I mutant, $n = 3$) LKB1. **e**, CPS1, LKB1 and phosphorylated acetyl-CoA carboxylase (pACC, S79) abundance upon LKB1 re-expression. **f**, CPS1, total and pACC abundance in A549, H2122 and H460 cells treated with the AMPK activator A769662. Statistical significance was assessed using a two-tailed Student's t-test (**c**) or one-way ANOVA followed by Tukey's multiple comparisons test (**d**). $^{**}P < 0.01$. TMA was performed once and all other experiments were repeated three times or more.

In the urea cycle, mitochondrial carbamoyl phosphate condenses with ornithine to produce citrulline, which is exported to the cytosol and converted into arginine (Fig. 1b). Although the cytosolic enzymes are broadly expressed, the mitochondrial enzymes, including CPS1, are largely confined to hepatocytes, restricting robust urea production from ammonia to the liver[5]. Somatic ASS1 and ASL loss in some tumour cells promotes proliferation by increasing aspartate availability for other pathways[6]. To assess the cytosolic segment, we deprived cells of arginine and measured growth in the presence and absence of exogenous citrulline. Arginine depletion suppressed growth of all lines, but KL cells were protected by the addition of citrulline, indicating that these cells are able to generate arginine from citrulline (Fig. 1d). Neither ornithine nor nitric oxide was protective, indicating that a complete cycle in KL cells is lacking and nitric oxide is not an essential by-product of this pathway in KL cells (Fig. 1d). KL cells were also not selectively sensitive to silencing of ornithine decarboxylase, which initiates conversion of ornithine to polyamines (Extended Data Fig. 4d).

We used orthogonal data from 94 lung cancer cell lines including 14 K, 16 L (loss of LKB1) and 9 KL lines (Supplementary Table 7) to examine the relationship between CPS1 and LKB1. Reversed-phase proteomics identified LKB1 as the most negatively correlated to *CPS1* mRNA among 176 proteins and phosphoproteins (Extended Data Fig. 4e and Supplementary Table 8). Transcriptome analysis covering 19,579 genes ranked *CPS1* as the second most inversely correlated mRNA with LKB1 protein (Fig. 2a and Supplementary Table 9). A human lung tumour tissue microarray detected CPS1 protein in 18% of samples, and tumours with intense or moderate CPS1 staining expressed little to no LKB1 protein (Fig. 2b and Extended Data Fig. 4f, g). In human lung adenocarcinoma, tumours with abundant *CPS1* mRNA were highly enriched for LKB1 loss (Fig. 2c). CPS1 was also expressed in patient-derived NSCLC xenografts, but only in LKB1-deficient tumours (Extended Data Fig. 4h). Abundant *CPS1* mRNA correlates with poor prognosis in NSCLC (Extended Data Fig. 4i).

To test whether LKB1 regulates CPS1 expression, we engineered KL cells to express wild-type or kinase-dead LKB1 (LKB1-WT or LKB1-KD). Expression of LKB1-WT but not LKB1-KD reduced CPS1 expression (Fig. 2d, e and Extended Data Fig. 5a–c), although as recently reported[7], neither silencing LKB1 nor activating AMPK in K cells altered CPS1 (Extended Data Fig. 5d). LKB1 induces metabolic effects through the fuel sensor AMPK[8,9]. In KL cells, pharmacological activation of AMPK or expression of constitutively active AMPK reduced CPS1 mRNA and protein, and silencing AMPK increased CPS1 expression even in the presence of LKB1 (Fig. 2f and Extended Data Fig. 5e–h). Although AMPK inhibits mTOR, neither inhibition nor activation of mTOR affected CPS1 expression (Extended Data Fig. 5i, j).

Chromatin immunoprecipitation (ChIP) followed by sequencing (ChIP–seq) data of the *CPS1* locus in A549 (KL) cells contained chromatin features consistent with an enhancer element in intron 1 (Extended Data Fig. 6a). ChIP–qPCR revealed markedly increased histone H3K27 acetylation, H3K4 trimethylation and RNA polymerase-II binding at this enhancer in KL compared to K cells, with AMPK activation reducing these signals (Extended Data Fig. 6b, c). FOXA1, CREB1 and TEAD4, three transcription factors repressed by AMPK[10–12], also displayed enhanced binding in KL cells, with binding inhibited upon AMPK activation (Extended Data Fig. 6b, c). Silencing of FOXA1 reduced CPS1 mRNA and protein (Extended Data Fig. 6d, e).

Next, NSCLC cell lines were transfected with CPS1-targeting or control short interfering RNAs (siRNAs). CPS1 silencing reduced viability in KL lines, but other cell lines, including L cells expressing CPS1, tolerated CPS1 silencing (Fig. 3a, b and Extended Data Fig. 7a, b). Among five KL cell lines, only A549 tolerated CPS1 silencing, although even these cells trended towards reduced viability (Extended Data Fig. 7c). Deleting CPS1 using CRISPR–Cas9 reduced KL cell viability (Extended Data Fig. 7d, e) and LKB1-WT protected KL cells against CPS1 silencing or knockout (Fig. 3c and Extended Data Fig. 7f). To control the timing of CPS1 silencing, we generated KL cells with doxycycline (Dox)-inducible expression of CPS1 short hairpin RNA (shRNA; shCPS1-1 and shCPS1-2) or *Renilla* luciferase shRNA as a control (shREN) (Extended Data Fig. 7g). In H460 (KL) cells, CPS1 depletion increased the doubling time,

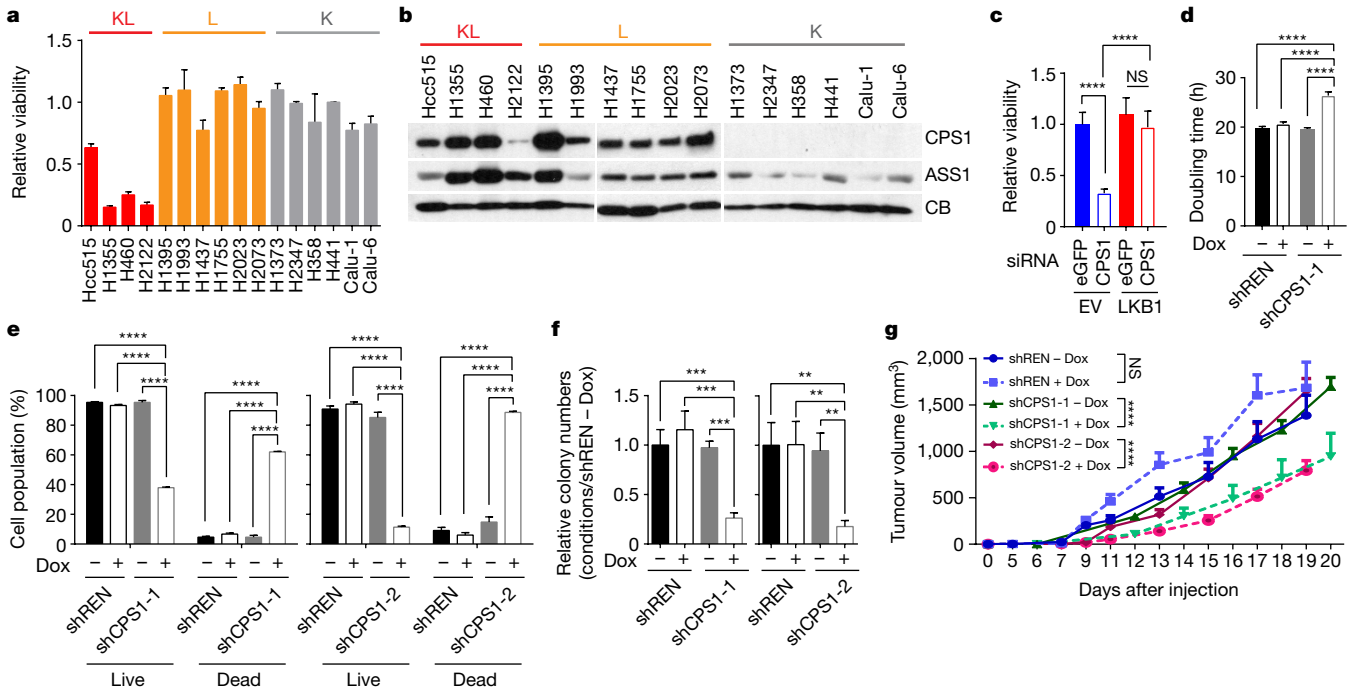

Figure 3 | KL cells and tumours require CPS1. a, Effect of *CPS1* silencing on KL, L and K cells (H1373 ($n=4$); H1437, H1755, H2023, H2073, H358 ($n=6$); other cell lines ($n=3$)). **b**, Abundance of CPS1 and another urea cycle enzyme, ASS1 in cells from **a**. CB, cyclophilin B (loading control). **c**, Effect of silencing *CPS1* on H460-EV and H460-LKB1-WT cells ($n=11$). **d**, Effects of a Dox-induced *CPS1* shRNA (shCPS1-1) on cell proliferation ($n=3$). shREN is a Dox-inducible control shRNA. **e**, Percentages of live and dead cells eight days after induction of CPS1-targeting (shCPS1-1, shCPS1-2) or control (shREN) shRNAs ($n=3$). **f**, Growth of anchorage-independent colonies 22 days after Dox induction ($n=3$). **g**, Growth of subcutaneous H460-derived xenografts in nude mice in the presence and absence of Dox (200 mg kg^{-1}) introduced one day after implantation. Mean tumour volume ± s.e.m. are shown for each group ($n=10$ tumours except for shCPS1-2 −Dox, where $n=8$). Data in **a**, **c**–**f** are the mean ± s.d. of three or more independent cultures. In **c**–**f**, statistical significance was assessed using a one-way ANOVA followed by Tukey's multiple comparisons test. In **g**, to calculate significance on repeated measurements over time, a two-way ANOVA was used. The mouse xenograft experiment was performed twice for shCPS1-1 ($n=5$ mice per experiment, total $n=10$) and once for shCPS1-2 and shREN ($n=10$). All other experiments were repeated three times or more. $^{**}P<0.01$; $^{***}P<0.001$; $^{****}P<0.0001$. NS, not significant.

induced cell death and suppressed colony formation in soft agar (Fig. 3d–f). An shRNA-resistant mouse *Cps1* cDNA protected viability (Extended Data Fig. 7h). Nude mice were injected subcutaneously with H460 cells expressing shREN, shCPS1-1 or shCPS1-2 and treated with or without Dox. Dox induction of shCPS1 reduced tumour growth and enhanced cell death (Fig. 3g and Extended Data Figs 7i, 8a). CPS1 silencing also suppressed growth of H2122 (KL) tumours (Extended Data Fig. 8b, c).

A potential explanation for the reliance of KL cells on CPS1 is a heightened requirement to detoxify ammonia. However, silencing CPS1 only marginally increased ammonia secretion (Extended Data Fig. 9a, b). Carbamoyl phosphate is also the initiating metabolite in pyrimidine synthesis. This pool of carbamoyl phosphate arises in the cytosol from CPS2, part of the trifunctional CAD enzyme (carbamoyl-phosphate synthetase 2, aspartate transcarbamoylase, and dihydroorotase) catalysing the first three steps of pyrimidine synthesis[13,14]. The enzymatic activity of CAD is distinct from CPS1, as it uses glutamine rather than ammonia as the nitrogen source. CAD abundance and activation as reported by S1859 phosphorylation[15] were unchanged between K and KL cells, and neither *CPS1* siRNAs nor CRISPR–Cas9 had off-target effects on CAD (Extended Data Fig. 9c, d). Analysis of the *CAD* genomic locus revealed no consistent differences in epigenetic features or FOXA1, CREB1 and TEAD4 binding between K and KL cells, and silencing these transcription factors did not alter CAD expression (Extended Data Fig. 10a–d). These findings indicate that *CPS1* and *CAD* transcription are regulated through distinct mechanisms.

Although mitochondrial and cytosolic carbamoyl phosphate generally function as distinct pools, germline deficiency of ornithine carbamoyltransferase (OTC) results in systemic pyrimidine accumulation, indicating that mitochondrial carbamoyl phosphate feeds pyrimidine synthesis under some circumstances[16]. CPS1 silencing in H460 cells resulted in pyrimidine depletion, purine accumulation and a decreased pyrimidine to purine ratio (Fig. 4a and Extended Data Fig. 9e). Furthermore, incubating cells with $^{15}NH_4^+$ revealed CPS1-dependent transfer of this nitrogen into thymidine, a pyrimidine nucleoside (Fig. 4b). Thus, KL cells use CPS1 to maintain pyrimidine pools.

Because disruption of the pyrimidine/purine balance impairs DNA replication[17,18], we examined cell cycle distribution during CPS1 silencing. 5-Bromodeoxyuridine (BrdU) incorporation and DNA content analysis revealed cellular accumulation in an ineffective S phase (less BrdU incorporation) (Extended Data Fig. 9f, g). G2/M accumulation also occurred in p53-competent H460 cells but not p53-mutant H2122 cells (Extended Data Fig. 9g). Prolonged inhibition of DNA replication induces double-stranded DNA breaks and cell death[19,20], suggesting a mechanism for CPS1 addiction. Indeed, CPS1-silenced cells and xenografts, but not shREN controls demonstrated increased histone H2AX phosphorylation (γH2AX S319) (Fig. 4c and Extended Data Fig. 9h, i), indicating that CPS1 is required to prevent double-stranded DNA breaks. Double-stranded DNA breaks associated with altered pyrimidine to purine ratios can result from replication-fork stalling[21], so we performed DNA fibre assays to monitor progression of individual DNA replication forks in the presence and absence of CPS1. Control cells incorporated 5-iodo-2′-deoxyuridine (IdU) and 5-chloro-2′-deoxyuridine (CldU) into long DNA tracks, but CPS1-silenced cells exhibited short tracks, indicating impairment of replication progression (Extended Data Fig. 9j). Supplementing CPS1-silenced cells with pyrimidine nucleosides but not purine nucleosides prevented γH2AX phosphorylation and rescued replication-fork stalling (Fig. 4d, e and Extended Data Fig. 10e). Pyrimidines but not purines also norma-

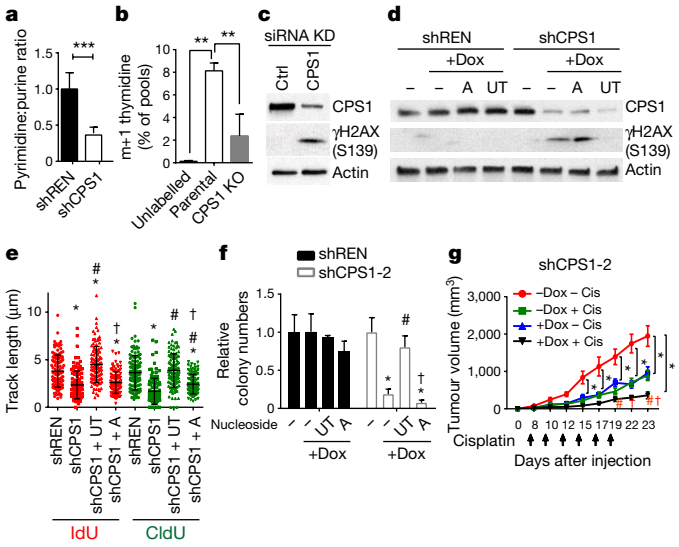

Figure 4 | *CPS1* silencing results in pyrimidine depletion, replication-fork stalling and DNA damage. a, Pyrimidine:purine ratio from data in Extended Data Fig. 9e. **b**, ^{15}N labelling in thymidine in control or CPS1-deficient (CRISPR–Cas9 knockout (KO)) H460 cells cultured with $^{15}NH_4Cl$ ($n = 3$). **c**, Abundance of CPS1 and phosphorylated histone H2AX (γH2AX) in H460 cells transfected with control or *CPS1*-targeting siRNA. **d**, Effect of supplementing uridine and thymidine (UT) or adenosine (A) on γH2AX abundance in *CPS1*-silenced H460 cells. **e**, Effect of uridine and thymidine or adenosine supplementation on DNA fibre lengths in *CPS1*-silenced cells. At least 112 tracks were measured for each condition. **f**, Effect of uridine and thymidine or adenosine supplementation on anchorage-independent growth ($n = 3$). **g**, Growth of H460 shCPS1-2 xenografts in the presence and absence of Dox with or without cisplatin (Cis). Arrows indicate days of injection with cisplatin. Mean tumour volume ± s.e.m. are shown for each group ($n = 8$). For experiments in cell lines, data are mean ± s.d. of three independent cultures. Significance was assessed using a two-tailed Student's *t*-test (**a**), one-way ANOVA with Tukey's multiple comparisons test (**b**, **e**, **f**) or two-way ANOVA with Tukey's multiple comparisons test (**g**). In **e**, $^*P < 0.05$ compared to shREN; $^\#P < 0.05$ compared to shCPS1; $^\dagger P < 0.05$ compared to shCPS1 and uridine and thymidine (UT). In **f**, $^*P < 0.05$ compared to no treatment; $^\#P < 0.05$ compared to +Dox with no nucleoside supplementation, $^\dagger P < 0.05$ compared to Dox and uridine and thymidine (UT). In **g**, $^*P < 0.05$ compared to −Dox and −Cis; $^\#P < 0.05$ compared to −Dox and +Cis; $^\dagger P < 0.05$ compared to +Dox and −Cis. In all other panels: $^{**}P < 0.01$; $^{***}P < 0.001$. Nucleotide measurements and DNA fibre assays were performed twice. All other experiments were repeated three times or more.

lized proliferation and colony formation in CPS1-silenced cells (Fig. 4f and Extended Data Fig. 10e–i). Finally, cisplatin, a DNA-damaging agent and first-line therapeutic in NSCLC, was combined with CPS1 silencing to reduce growth of KL tumours (Fig. 4g and Extended Data Fig. 10j, k).

Cancer cells reprogram metabolism to support survival and proliferation, and particular oncogenic genotypes impose specific vulnerabilities[22]. Because both KRAS and LKB1 regulate metabolism, co-mutation of the two genes might specify metabolic phenotypes not observed with either mutation alone, perhaps contributing to the aggressive oncological behaviour of co-mutant tumours. In mice, co-mutation of KRAS and LKB1 in lung tumours imposes a state of dependence on enzymes involved in conventional pyrimidine biosynthesis[3]. The surprising requirement of CPS1, a urea cycle enzyme, to maintain the purine/pyrimidine balance in human KL cells implies that this enzyme provides an alternative pool of carbamoyl phosphate to maintain pyrimidine availability. Disrupting this balance by reducing the contribution of CPS1 to pyrimidine metabolism severely altered DNA-polymerase processivity, resulting in DNA damage and cell death. The fact that L cells with wild-type KRAS express, but do not require, CPS1 suggests that the metabolic effects of oncogenic KRAS are essential for CPS1 addiction. It is interesting that oncogenic KRAS stimulates glutamine catabolism in the mitochondria[23], perhaps creating a local supply of ammonia for CPS1 while reducing glutamine availability for CAD-mediated pyrimidine biosynthesis in the cytosol (Extended Data Fig. 1a). Our findings suggest the use of CPS1 or related pathway components as therapeutic targets in KL mutant lung adenocarcinomas, providing both enrollment biomarkers (KL oncogenic genotype plus CPS1 expression) and a new mechanism of oncogene addiction.

Online Content Methods, along with any additional Extended Data display items and Source Data, are available in the online version of the paper; references unique to these sections appear only in the online paper.

Received 24 June 2016; accepted 10 April 2017.
Published online 24 May 2017.

1. Calles, A. *et al.* Immunohistochemical loss of LKB1 is a biomarker for more aggressive biology in *KRAS*-mutant lung adenocarcinoma. *Clin. Cancer Res.* **21,** 2851–2860 (2015).
2. Ji, H. *et al.* LKB1 modulates lung cancer differentiation and metastasis. *Nature* **448,** 807–810 (2007).
3. Liu, Y. *et al.* Metabolic and functional genomic studies identify deoxythymidylate kinase as a target in *LKB1*-mutant lung cancer. *Cancer Discov.* **3,** 870–879 (2013).
4. Kim, H. S. *et al.* Systematic identification of molecular subtype-selective vulnerabilities in non-small-cell lung cancer. *Cell* **155,** 552–566 (2013).
5. Liu, H., Dong, H., Robertson, K. & Liu, C. DNA methylation suppresses expression of the urea cycle enzyme carbamoyl phosphate synthetase 1 (CPS1) in human hepatocellular carcinoma. *Am. J. Pathol.* **178,** 652–661 (2011).
6. Rabinovich, S. *et al.* Diversion of aspartate in ASS1-deficient tumours fosters *de novo* pyrimidine synthesis. *Nature* **527,** 379–383 (2015).
7. Celiktas, M. *et al.* Role of CPS1 in cell growth, metabolism, and prognosis in LKB1-inactivated lung adenocarcinoma. *J. Natl. Cancer Inst.* **109,** 1–9 (2016).
8. Shackelford, D. B. & Shaw, R. J. The LKB1–AMPK pathway: metabolism and growth control in tumour suppression. *Nat. Rev. Cancer* **9,** 563–575 (2009).
9. Hardie, D. G., Ross, F. A. & Hawley, S. A. AMPK: a nutrient and energy sensor that maintains energy homeostasis. *Nat. Rev. Mol. Cell Biol.* **13,** 251–262 (2012).
10. Mo, J.-S. *et al.* Cellular energy stress induces AMPK-mediated regulation of YAP and the Hippo pathway. *Nat. Cell Biol.* **17,** 500–510 (2015).
11. Sun, Y. *et al.* Metformin induces apoptosis of human hepatocellular carcinoma HepG2 cells by activating an AMPK/p53/miR-23a/FOXA1 pathway. *Onco Targets Ther.* **9,** 2845–2853 (2016).
12. Kim, H. G. *et al.* Metformin inhibits P-glycoprotein expression via the NF-κB pathway and CRE transcriptional activity through AMPK activation. *Br. J. Pharmacol.* **162,** 1096–1108 (2011).
13. Chen, K. C., Vannais, D. B., Jones, C., Patterson, D. & Davidson, J. N. Mapping of the gene encoding the multifunctional protein carrying out the first three steps of pyrimidine biosynthesis to human chromosome 2. *Hum. Genet.* **82,** 40–44 (1989).
14. Simmer, J. P. *et al.* Mammalian dihydroorotase: nucleotide sequence, peptide sequences, and evolution of the dihydroorotase domain of the multifunctional protein CAD. *Proc. Natl Acad. Sci. USA* **87,** 174–178 (1990).
15. Ben-Sahra, I., Howell, J. J., Asara, J. M. & Manning, B. D. Stimulation of *de novo* pyrimidine synthesis by growth signaling through mTOR and S6K1. *Science* **339,** 1323–1328 (2013).
16. Wraith, J. E. Ornithine carbamoyltransferase deficiency. *Arch. Dis. Child.* **84,** 84–88 (2001).
17. Poli, J. *et al.* dNTP pools determine fork progression and origin usage under replication stress. *EMBO J.* **31,** 883–894 (2012).
18. Anglana, M., Apiou, F., Bensimon, A. & Debatisse, M. Dynamics of DNA replication in mammalian somatic cells: nucleotide pool modulates origin choice and interorigin spacing. *Cell* **114,** 385–394 (2003).
19. Petermann, E., Orta, M. L., Issaeva, N., Schultz, N. & Helleday, T. Hydroxyurea-stalled replication forks become progressively inactivated and require two different RAD51-mediated pathways for restart and repair. *Mol. Cell* **37,** 492–502 (2010).
20. Labib, K. & Hodgson, B. Replication fork barriers: pausing for a break or stalling for time? *EMBO Rep.* **8,** 346–353 (2007).
21. Reichard, P. Interactions between deoxyribonucleotide and DNA synthesis. *Annu. Rev. Biochem.* **57,** 349–374 (1988).
22. Shackelford, D. B. *et al.* LKB1 inactivation dictates therapeutic response of non-small cell lung cancer to the metabolism drug phenformin. *Cancer Cell* **23,** 143–158 (2013).
23. Son, J. *et al.* Glutamine supports pancreatic cancer growth through a KRAS-regulated metabolic pathway. *Nature* **496,** 101–105 (2013).

Supplementary Information is available in the online version of the paper.

Acknowledgements We thank A. Jaffe and members of the DeBerardinis laboratory for critiquing the manuscript and J. Kozlitina for statistical expertise. R.J.D. is supported by grants from the NIH (R01CA157996), Cancer Prevention and Research Institute of Texas (CPRIT RP130272), Robert A. Welch Foundation (I1733) and H.H.M.I. (Faculty Scholars Program). J.K. is supported by an American Lung Association Senior Research Training Fellowship (RT-306212). D.H.C. is supported by NIH grant (1R01CA196912). J.D.M., J.R.C., P.V. and I.W. are supported by the University of Texas Lung Specialized Programs of Research Excellence (SPORE) grant (P50CA70907). J.D.M. is also supported by NIH grant CA176284 and CPRIT grants RP120732 and RP110708.

Author Contributions J.K. and R.J.D. designed the study and wrote the paper. Z.H. performed the metabolomics. L.C. and M.N. provided biostatistics expertise. E.C. provided advice about replication-fork stalling. K.L. and J.X. performed ChIP–qPCR and provided advice on epigenetics. E.W., J.V. and D.L. provided human NSCLC samples for metabolomics. K.U.-K. and L.G. provided expertise in metabolomics and transcript analysis. C.G.P., D.H.C., P.V., J.R.-C. and I.W. performed tumour microarrays. Y.-F.L. and B.P.C.C. performed DNA fibre assays. B.F. provided expertise on AMPK. D.B. performed transient gene silencing. L.A.B. and J.V.H. provided reverse-phase proteomics and patient survival data. K.E.H. and J.D.M. provided cell lines, gene expression data and intellectual input regarding molecular lung cancer subtypes.

Author Information Reprints and permissions information is available at www.nature.com/reprints. The authors declare competing financial interests: details are available in the online version of the paper. Readers are welcome to comment on the online version of the paper. Publisher's note: Springer Nature remains neutral with regard to jurisdictional claims in published maps and institutional affiliations. Correspondence and requests for materials should be addressed to R.J.D. (Ralph.Deberardinis@UTSouthwestern.edu).

METHODS

Cell lines, culture and reagents. All NSCLC cell lines (A549, H1355, H157, H2122, Hcc515, H460, H1395, H1437, H1755, H1993, H2023, H2073, H1373, H2347, H358, H441, Calu-1 and Calu-6) used in this study were obtained from the Hamon Cancer Center Collection (University of Texas–Southwestern Medical Center). Cells were maintained in RPMI-1640 supplemented with penicillin–streptomycin, and 5% fetal bovine serum (FBS) at 37 °C in a humidified atmosphere containing 5% CO_2 and 95% air. All cell lines have been DNA fingerprinted for provenance using the PowerPlex 1.2 kit (Promega) and were mycoplasma-free using the e-Myco kit (Boca Scientific). H460-EV, H460-LKB1-WT and H460-LKB1-KD were generated by infecting H460 cells with pBABE retroviral vectors expressing no cDNA or cDNAs encoding wild-type or kinase-dead (K78I mutant) LKB1, respectively. pBABE-FLAG-LKB1-WT and -KD were from L. Cantley (Addgene plasmid 8592 and 8593, respectively) and pAMPK alpha2 delta312X (constitutively active AMPK) was from M. Birnbaum (Addgene plasmid 60127). For mouse CPS1 (mCPS1) cloning, mCPS1 cDNA was purchased from GE healthcare (cloneID 40098767), and subcloned into pWPXL lentiviral plasmid (Addgene, plasmid 12257). Stable integrants were sorted by flow cytometry (FACS Aria II SORP) for further analyses. To generate H460-shREN and -shCPS1 cells, parental H460 cells were infected by TRMPVIR retroviral vectors expressing Tet-shRNA targeting *Renilla* luciferase (REN) as negative control or Tet-shRNAs targeting CPS1, and stable integrants were obtained by flow cytometry (FACS Aria II SORP). The primers used to generate shCPS1 constructs were as follows: shCPS1-1 forward, 5′-TGCTGTTGACAGTGAGCGCAACCAAGGATGTCAAAGTGTATAGTGAAGCCACA-3′, shCPS1-2 forward, 5′-TGCTGTTGACAGTGAGCGCACCAAGGATGTCAAAGTGTACTAGTGAAGCCACA-3′.

All nucleosides (uridine, thymidine and adenosine), citrulline, ornithine and $NaNO_2$ were purchased from Sigma-Aldrich. Doxycycline was from Research Products International (RPI), Torin 1 and cisplatin were from Selleckchem and A769662 was from Tocris Bioscience.

Metabolomics. NSCLC cell lines were plated at $3–5 \times 10^6$ cells per 10-cm plate for 16 h before collection. Two hours before collection, cells were incubated with fresh media. At the time of collection, cells were washed with ice-cold saline, lysed with 80% methanol in water and quickly scraped into an Eppendorf tube followed by three freeze–thaw cycles in liquid nitrogen. The insoluble material was pelleted in a cooled centrifuge (4 °C) and the supernatant was transferred to a new tube and evaporated to dryness using a SpeedVac concentrator (Thermo Savant). Metabolites were reconstituted in 100 μl of 0.03% formic acid in LCMS-grade water, vortex-mixed and centrifuged to remove debris. For human NSCLC metabolomics, frozen tissues were weighed and divided into 3–9 fragments (around 3 mg per fragment) for technical replicates. Fragments were homogenized in 80% methanol in water and centrifuged at 14,000*g* for 15 min (4 °C). The supernatant was transferred to a new tube and evaporated to dryness as described above for cell lysates. Samples were randomized and blinded before analysing by LC–MS/MS. LC–MS/MS and data acquisition were performed using an AB QTRAP 5500 liquid chromatography/triple quadrupole mass spectrometer (Applied Biosystems SCIEX) as described previously[24] with an injection volume of 20 μl. Carbamoyl phosphate was detected in negative mode by monitoring ions 140 and 79 in Q1 and Q3, respectively. Chromatogram review and peak area integration were performed using MultiQuant software version 2.1 (Applied Biosystems SCIEX), and the peak area for each detected metabolite was normalized against the total ion count of that sample to correct for any variations introduced by sample handling through instrument analysis. The normalized areas were used as variables for the multivariate and univariate statistical data analysis. All multivariate analyses and modelling on the normalized data were carried out using Metaboanalyst 3.0 (http://www.metaboanalyst.ca). Univariate statistical differences of the metabolites between two groups were analysed using a two-tailed Student's *t*-test.

$^{15}NH_4$ labelling. Cells were plated at 24×10^6 cells per $2 \times$ 15-cm plate for 16 h before labelling. The next day, cells were incubated in labelling media containing 10 mM $^{15}NH_4Cl$ for 4 h before collection. At the time of collection, the cells were washed with ice-cold saline, lysed with 40% methanol:40% acetonitrile:20% water with 0.1 M formic acid and processed as described above (Metabolomics). Metabolites were reconstituted in 100 μl of 0.1% formic acid in LCMS-grade water, vortex-mixed and centrifuged to remove debris. Samples were randomized and blinded before analysing by LC–MS/MS. LC–MS/MS and data acquisition were performed as described previously on an AB SCIEX QTRAP 5500 (ref. 24) with slight modifications. In brief, the mobile phases used were 0.1% formic acid in water (A) and 0.1% formic acid in acetonitrile (B). The gradient program was as follows: 0–3 min, 0% B; 3–4 min, 0%–100% B; 4–5 min, 100% B; 5–5.1 min, 100%–0% B; 5.1–6 min, 0% B. The column was maintained at 35 °C and the samples were kept in the autosampler at 4 °C. The flow rate was 0.5 ml min^{-1} and the injection volume was 20 μl. Sample analysis was performed in positive mode. Declustering potential (DP), collision energy (CE) and collision cell exit potential (CXP) were optimized by direct infusion of reference standards using a syringe pump before sample analysis. Q1, Q3, DP, CE, CXP, retention time and dwell time for each transition of thymidine are in Supplementary Table 10. The MRM MS/MS detector conditions were set as follows: curtain gas 30 psi; ion spray voltages 1,200 V; temperature 650 °C; ion source gas 1, 50 psi; ion source gas 2, 50 psi; interface heater on; entrance potential 10 V. Dwell time for each transition was set at 3 ms. Samples were analysed in a randomized order, and MRM data was acquired using Analyst 1.6.1 software (Applied Biosystems SCIEX).

Metabolic assays. To measure NOS activity, 10,000 cells were cultured in a 96-well plate for 16 h before the assay, and free NO was quantified with a spectrophotometric assay (Sigma-Aldrich). For ammonia secretion, cells were cultured in fresh RPMI for 6 h and ammonia was measured with a spectrophotometric assay (Megazyme). In this assay, glucose deprivation induces ammonia secretion[25] and was used as a positive control for the effect of *CPS1* silencing on ammonia secretion in Extended Data Fig. 9b. For arginine deprivation and metabolite rescue experiments (citrulline, ornithine and $NaNO_2$), NSCLC cells were plated in 96-well plates at 3,000–5,000 cells per well. The following day, the culture medium was changed either to complete RPMI or arginine-depleted RPMI with or without 1 mM citrulline, 1 mM ornithine or 3 mM $NaNO_2$. Cell viability was assayed three days later using CellTiter-Glo (Promega).

Cell growth, cell death and viability. To monitor proliferation in a monolayer culture, $1–3 \times 10^5$ cells were seeded in a 6-cm dish. Every three days, cells were trypsinized and counted with a haemocytometer. The live cell content was estimated using a CellTiter-Glo assay (Promega). To examine cell death, cells were treated as indicated in the figure legend and stained with propidium iodide or with Annexin-V–FITC and propidium iodide. Cells were then analysed by flow cytometry (FACS Aria II SORP).

Soft-agar colony-formation assay. Four days after Dox induction, cells (1,000 per well) were suspended in 0.375% agar (Noble agar, Difco) pre-equilibrated with growth medium, over a 0.75% bottom agar layer in each well of a 6-well plate. Colonies were allowed to form for 20–22 days with intermittent medium supplementation (a few drops twice a week). Images were acquired with G box-Syngene (Syngene) and colonies were detected with GeneTools software (Syngene).

BrdU incorporation assay. Cells were labelled with BrdU labelling (10 μM) for 1 h followed by fixation. Incorporated BrdU was detected by immunostaining and quantified by FACS analysis.

DNA fibre assay. Cells were labelled with 100 μM iododeoxyuridine (IdU) for 10 min, then with 100 μM chlorodeoxyuridine (CldU) for 20 min. DNA fibres were spread as described previously[26] and stained with primary antibodies (mouse anti-BrdU/IdU from BD Bioscience; rat anti-BrdU/CldU from Accurate Chemical) and fluorescence-conjugated secondary antibodies (Alexa Fluor 488-anti-rat and Texas-Red-conjugated anti-mouse from Invitrogen). Fibres were imaged using Zeiss Axio Imager M2 and measured using AxioVision software (SE64 version 4.9.1).

qRT–PCR. RNA was extracted in TRIzol (Invitrogen) and isolated according to the manufacturer's protocol. cDNA was generated using the iScript synthesis kit (Bio-Rad), and abundance was measured on a Thermo qPCR instrument. Data were normalized to β-actin (*ACTB*) or *GAPDH*. Primers used for qRT–PCR were as follows: *CPS1* forward, 5′-ATTCCTTGGTGTGGCTGAAC-3′, reverse, 5′-ATGGAAGAGAGGCTGGGATT-3′; *ARG2* forward, 5′-GAGAAGCTGGCTTGATGAAA-3′, reverse, 5′-CAGCTCTGCTAACCACCTCA-3′; *ASS1* forward, 5′-CTGATGGAGTACGCAAAGCA-3′, reverse, 5′-CTCGAGAATGTCAGGGGTGT-3′; *ADC* forward, 5′-CCTCAGGCCTATGCTCAGTC-3′, reverse, 5′-CTGAGTTGATCACGGAAGCA-3′; *AGMAT* forward, 5′-CGACCTTGGATCCCTACAGA-3′, reverse, 5′-ACCAGCAATTTCAGGTGTCC-3′; *CAD* forward, 5′-TCAAGGTGACCCAGCACCTG-3′, reverse, 5′-TCAGGCAAAGGGATGCCCAA-3′; actin forward, 5′-AGAGCTACGAGCTGCCTGAC-3′, reverse, 5′-AGCACTGTGTTGGCGTACAG-3′, *GAPDH* forward, 5′-ACCCAGAAGACTGTGGATGG-3′, reverse, 5′-TTCAGCTCAGGGATGACCTT-3′.

RNA interference (RNAi). Transient gene-silencing experiments were performed with endoribonuclease-prepared siRNAs (esiRNA, Sigma-Aldrich) for *CPS1* and *CAD*, and with ON-TARGETplus-SMART pools (Dharmacon) for *LKB1*, *CREB1*, *FOXA1*, *TEAD4*, *ODC*, *TSC-1* and *TSC-2*, AMPKα-1 (*PRKAA1*) and AMPKα-2 (*PRKAA2*). In brief, siRNA oligos were transfected into cells with RNAiMAX transfection reagent (Invitrogen); esiRNA oligos targeting eGFP or siRNA universal negative controls were used as a negative control (Sigma-Aldrich). For Extended Data Figs 6e, 10d, triple transfections were performed (every other day, repeated three times) and western blots were assayed 144 h after the first transfection. Viability assays were performed after 96 h and cell death analyses and all other western blots were performed after 48 h. BrdU incorporation was measured after 24 h in H460 cells and after 36 h in H2122 cells. For inducible RNAi experiments, shREN and shCPS1-1 and shCPS1-2 were induced using doxycycline concentrations of 1.0–2.0 mg ml^{-1}.

ChIP–qPCR. ChIP experiments were performed as described[27] with modifications. In brief, around $1–2 \times 10^7$ cells were crosslinked with 1% formaldehyde for 5 min

at room temperature. Chromatin was sonicated to around 500 bp in RIPA buffer (10 mM Tris-HCl, 1 mM EDTA, 0.1% sodium deoxycholate, 0.1% SDS, 1% Triton X-100, 0.25% sarkosyl, pH 8.0) with 0.3 M NaCl. Sonicated chromatin samples were incubated with 5 μg antibody at 4 °C. After overnight incubation, protein A or G Dynabeads (Invitrogen) were added to the ChIP reactions and incubated for four additional hours at 4 °C to collect the immunoprecipitated chromatin. Subsequently, Dynabeads were washed twice with 1 ml of RIPA buffer, twice with 1 ml of RIPA buffer with 0.3 M NaCl, twice with 1 ml of LiCl buffer (10 mM Tris-HCl, 1 mM EDTA, 0.5% sodium deoxycholate, 0.5% NP-40, 250 mM LiCl, pH 8.0), and twice with 1 ml of TE buffer (10 mM Tris-HCl, 1 mM EDTA, pH 8.0). The chromatin was eluted in SDS elution buffer (1% SDS, 10 mM EDTA, 50 mM Tris-HCl, pH 8.0) followed by reverse crosslinking at 65 °C overnight. ChIP DNA were treated with RNaseA (5 μg ml^{-1}) and protease K (0.2 mg ml^{-1}) and purified using QIAquick Spin Columns (Qiagen). The purified ChIP DNA was quantified by real-time PCR using the iQ SYBRGreen Supermix (Bio-Rad). The following antibodies were used: H3K27ac (Abcam, ab4729), H3K4me3 (Millipore, 04-745,), RNAPII (Santa Cruz Biotechnology, sc-899), FOXA1 (Abcam, ab23738), TEAD4 (Abcam, ab58310), CREB1 (Santa Cruz Biotechnology, sc-186) and IgG (Millipore, 12-370). Other ChIP–seq datasets were obtained from previous publications or the ENCODE project. Primers used for *CPS1* qPCR were as follows: control forward, 5′-AAACCCACGTCCAGCACAGTGTC-3′, reverse, 5′-AATAGCGGGTAAGGATGTAGACAGG-3′; promoter forward, 5′-TTAACCCACCCGGACAAAGAGG-3′, reverse, 5′-AATAGCCCTTCTGTTA CTGTCC-3′; enhancer 1 forward, 5′-CCTGCCCTATGACTCAACTTAC-3′, reverse, 5′-GGAAATCGGAAATAGGACCCGTGC-3′; enhancer 2 forward, 5′-CCACATGCTTCTCTGTGATCCTC-3′, reverse, 5′-ATTCTAAAGAGCA ACCCTAGCTG-3′. Primers used for *CAD* qPCR were as follows: promoter 1 forward, 5′-TCCTTCCCGCTTCTCCGTACTCG-3′, reverse, 5′-CACAGAG TGGGATAAGGTCTGC-3′; promoter 2 forward, 5′-AGCCCAGCCCTGCTTC TTTCTTGC-3′, reverse, 5′-GGGATGCCATAGTTGCCGATCAGAG-3′.

CRISPR–Cas9-mediated recombination. CPS1-deficient H460 clones for isotope tracing were generated using the original CRISPR–Cas9 system[28] and pools for cell viability assays were generated using the lentiCRISPR V2 system[29]. To control for variations among individual clones in the tracing experiments, 4–5 clones were pooled together. Guide-RNA oligos were as follows:

forward, 5′-CACCG ACAATGGCCAACCCTATTAT-3′, reverse, 5′-AAACATA ATAGGGTTGGCCATTGTC-3′.

Western blot analysis. Protein lysates were prepared in either RIPA or CHAPS buffer and quantified using the BCA protein assay (Thermo Scientific). Proteins were separated on 4–20% SDS–PAGE gels, transferred to PVDF membranes, and probed with antibodies against CPS1 (Abcam, ab3682), β-actin (Abcam, ab8227), ASS1 (clone 2B10, Abcam, ab124465), cyclophilin B (clone EPR12703(B), Abcam, ab178397), total AMPK (Cell Signaling, 2603), pAMPK (Cell signaling, 2531), total ACC (Cell Signaling, 3662), pACC (Cell Signaling, 11818), LKB1 (Cell Signaling, 3050), γH2AX (Cell Signaling, 9718), total CAD (Cell Signaling, 11933), pCAD (Cell Signaling, 12662), NOS3 (BD, 610298), pS6 (Cell Signaling, 2211), p4E-BP1 (Cell Signaling, 2855), CREB1 (Santa Cruz, sc-186X), FOXA1 (ab23738), TEAD4 (ab58310).

Xenografts. Animal procedures were performed with the approval of the UT Southwestern IACUC. Tumour size must not exceed 20 mm at the largest diameter and this tumour threshold was never exceeded in any experiment. H460 shREN or shCPS1-1 and shCPS1-2 cells were suspended in RPMI (10^7 per ml), mixed 1:1 with Matrigel (Becton Dickinson), and 10^5 cells for H460 and 10^6 cells for H2122 were implanted subcutaneously into 6-week-old NCRNU mice. After tumour cell injection, mice were randomized and then allocated into cages. Mice were fed regular chow or doxycycline-containing chow (200 mg kg^{-1}, Bio-Serv), starting one day after implantation. For cisplatin treatment, tumour-bearing mice were intraperitoneally injected with cisplatin at 2 mg kg^{-1} or PBS when the xenografted tumours measured around 100 mm^3. Injections were performed every other day for a total of 5–6 doses. Tumour size was measured every other day with electronic callipers. Tumour volumes were calculated every 3–4 days by calliper measurements of the short (a) and long (b) tumour diameters (volume $= a^2 \times b / 2$) or of tumour height (h), short (a) and long (b) tumour width (volume $= h \times a \times b / 2$) depending on tumour shape.

Tissue γH2AX staining. Paraffin-embedded tumour sections from mouse xenografts were deparaffinized with xylene followed by ethanol rehydration, fixed in 4% paraformaldehyde and antigens were retrieved with 10 mM sodium citrate pH 6.0. Sections were then subjected to endogenous peroxidase blocking with 0.3% H_2O_2. Bovine serum albumin (BSA, 3%) in 0.1% PBST was used as the blocking agent and antibody dilution solution. After 1 h blocking, samples were incubated overnight at 4 °C with the primary antibody (Cell Signaling, 9718) followed by incubation with fluorescence-conjugated secondary antibodies (ThermoFisher Scientific, A-21206). Images were acquired as a series of 0.4-μm stacks with a DeltaVision system (Applied Precision). Raw images were deconvolved using the iterative algorithm implemented in the softWoRx software (Applied Precision).

TUNEL assay. Cell death was detected in xenografts using the *In Situ* Cell Death Detection kit, Fluorescein (Sigma-Aldrich) according to the manufacturer's protocol. In brief, tissue sections were deparaffinized with xylene and rehydrated with ethanol, then treated with proteinase K (5 μg ml^{-1}, New England Biolabs). After washing in PBS, sections were incubated with reaction solution for 1 h at 37 °C in a humidified atmosphere in the dark. Images were acquired with an Olympus IX81 microscope.

Human Lung Cancer Tissue Microarray. A tissue microarray with 180 human NSCLC samples (MD Anderson Cancer Center) was probed with antibodies against CPS1 (Sigma-Aldrich, HPA021400) and LKB1 (Cell Signaling, 13752). Immunocytochemistry was performed in a Leica Bond Max (Leica Biosystem) with an antibody dilution at 1:800 for CPS1 and 1:250 for LKB1. Liver tissue was used as a control. Staining intensity was graded as: 0 (no staining); 1+ (weak staining); 2+ (moderate staining); and 3+ (intense staining) by one pathologist, then reviewed by a second pathologist independently. The percentage of stained tumour cells was recorded, and the *H*-score was assigned using the following formula: $1 \times$ (% cells 1+) $+ 2 \times$ (% cells 2+) $+ 3 \times$ (% cells 3+). A final *H*-score of 0 was assigned as negative; 1–100 as weak; 101–200 as medium; and 201–300+ as strong.

Patient survival data. Differences in survival based on either *LKB1* mutation or *CPS1* mRNA expression was determined in lung adenocarcinoma tumours from The Cancer Genome Atlas (TCGA) (TCGA LUAD provisional). The analysis was restricted to the 230 tumours that had undergone both whole-exome sequencing and mRNA profiling. Methods for data generation, normalization and bioinformatics analyses were previously described in the TCGA LUAD publication[30]. For the present analysis, data from this cohort was downloaded and analysed using cBioPortal (www.cbioportal.org). mRNA data used for this analysis was RNA Seq V2 RSEM with a *z*-score threshold of 2.0 applied to identify tumours with high levels of *CPS1* upregulation.

Statistical analysis. No statistical methods were used to predetermine sample size. Metabolomics and flux analysis samples were randomized before LC–MS/MS analysis. For xenograft experiments, mice injected with tumour cells were randomized before being allocated to cages. All other experiments were not randomized, and the investigators were not blinded to allocation during experiments or to outcome assessment. Experiments in Figs 1a, 2b, 3g with shREN and shCPS1-2, Extended Data Figs 1c, 2, 7i, 8c, 9i, 10j, k were performed once, and experiments in Figs 1d, 3g with shCPS1-1, Fig. 4e, g with shCPS1-2 and Extended Data Figs 6b, 7f, 9e, j, 10b were performed twice. All other experiments were performed three times or more. Variation for xenograft tumour volume is indicated using the standard error of the mean, and variation in all other experiments is indicated using the standard deviation. To assess the significance of differences between two conditions, a two-tailed Welch's unequal variances *t*-test was used. Where the data points showed a skewed distribution (for example, Extended Data Fig. 1c), a Wilcoxon signed-rank test was performed. For comparisons among three or more groups, a one-way ANOVA followed by Tukey's multiple comparisons test was performed. To examine significance in xenograft tumour growth between two or among three or more groups, a two-way ANOVA followed by Tukey's multiple comparisons test was performed. Before applying an ANOVA, we first tested whether there was homogeneity of variation among the groups (as required for ANOVA) using the Brown–Forsythe test. In all xenograft assays, we injected 6–7-week-old NCRNU mice (both male and female), 10 mice per treatment (except Extended Data Fig. 10j, k: $n = 4$ per group), as we expected based on previous pilot experiments to observe differences in tumour size after two weeks. When mice died before the end of experiments, data from those mice were excluded (Fig. 3g for shCPS1-2 −Dox).

Data availability. All primary data are included in the Source Data associated with each figure accompanying this Letter. Any additional information required to interpret, replicate or build upon the Methods or findings reported in the manuscript are available upon request from the corresponding author.

24. Mullen, A. R. *et al.* Oxidation of alpha-ketoglutarate is required for reductive carboxylation in cancer cells with mitochondrial defects. *Cell Rep.* **7,** 1679–1690 (2014).
25. Yang, C. *et al.* Glioblastoma cells require glutamate dehydrogenase to survive impairments of glucose metabolism or Akt signaling. *Cancer Res.* **69,** 7986–7993 (2009).
26. Jackson, D. A. & Pombo, A. Replicon clusters are stable units of chromosome structure: evidence that nuclear organization contributes to the efficient activation and propagation of S phase in human cells. *J. Cell Biol.* **140,** 1285–1295 (1998).
27. Huang, J. *et al.* Dynamic control of enhancer repertoires drives lineage and stage-specific transcription during hematopoiesis. *Dev. Cell* **36,** 9–23 (2016).
28. Ran, F. A. *et al.* Genome engineering using the CRISPR–Cas9 system. *Nat. Protoc.* **8,** 2281–2308 (2013).
29. Shalem, O. *et al.* Genome-scale CRISPR–Cas9 knockout screening in human cells. *Science* **343,** 84–87 (2014).
30. Cancer Genome Atlas Research Network. Comprehensive molecular profiling of lung adenocarcinoma. *Nature* **511,** 543–550 (2014).

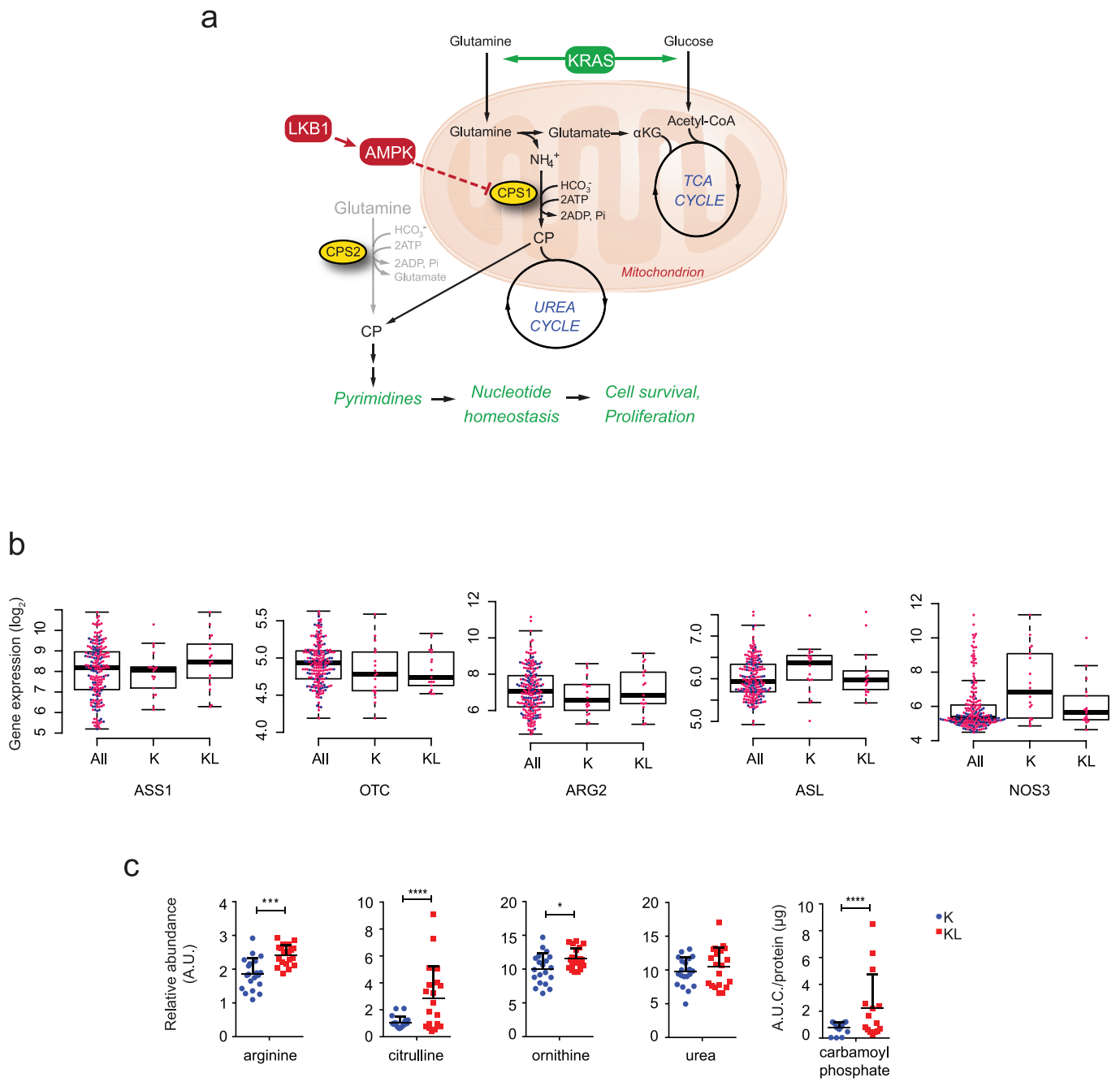

Extended Data Figure 1 | Altered urea cycle metabolism in KL cells. **a**, Illustration of the urea and tricarboxylic acid (TCA) cycle. Metabolic alterations mediated by concurrent mutations of KRAS and LKB1 render cells dependent on CPS1 for pyrimidine synthesis. Generally, mitochondrial and cytosolic carbamoyl phosphate are thought to follow distinct metabolic routes into the urea cycle and pyrimidine biosynthesis, respectively. In KL cells, however, CPS1 supports nucleotide homeostasis by providing an alternative supply of carbamoyl phosphate for *de novo* pyrimidine synthesis. Dependence on CPS1 is exacerbated by mutant KRAS, perhaps because of the effects of this oncogene on the metabolism of glutamine and other nutrients in the mitochondria. αKG, α-ketoglutaric acid; CP, carbamoyl phosphate. **b**, Distribution of mRNA abundance of urea cycle-related enzymes in 203 cell lines. Pink dots are cancer cell lines and blue dots are bronchial or small airway epithelial cell lines. Statistical significance was assessed using a two-tailed Student's *t*-test. Abundance data are in Supplementary Table 6. **c**, Abundance of urea cycle intermediates in the same cell lines used in Fig. 1a. Individual data points are shown as mean ± s.d. for three (carbamoyl phosphate) or four (all others) independent cultures. Statistical significance for citrulline and carbamoyl phosphate was assessed using a Wilcoxon signed-rank test. Other data were assessed using two-tailed Student's *t*-tests. $^{*}P < 0.05$; $^{***}P < 0.001$; $^{****}P < 0.0001$.

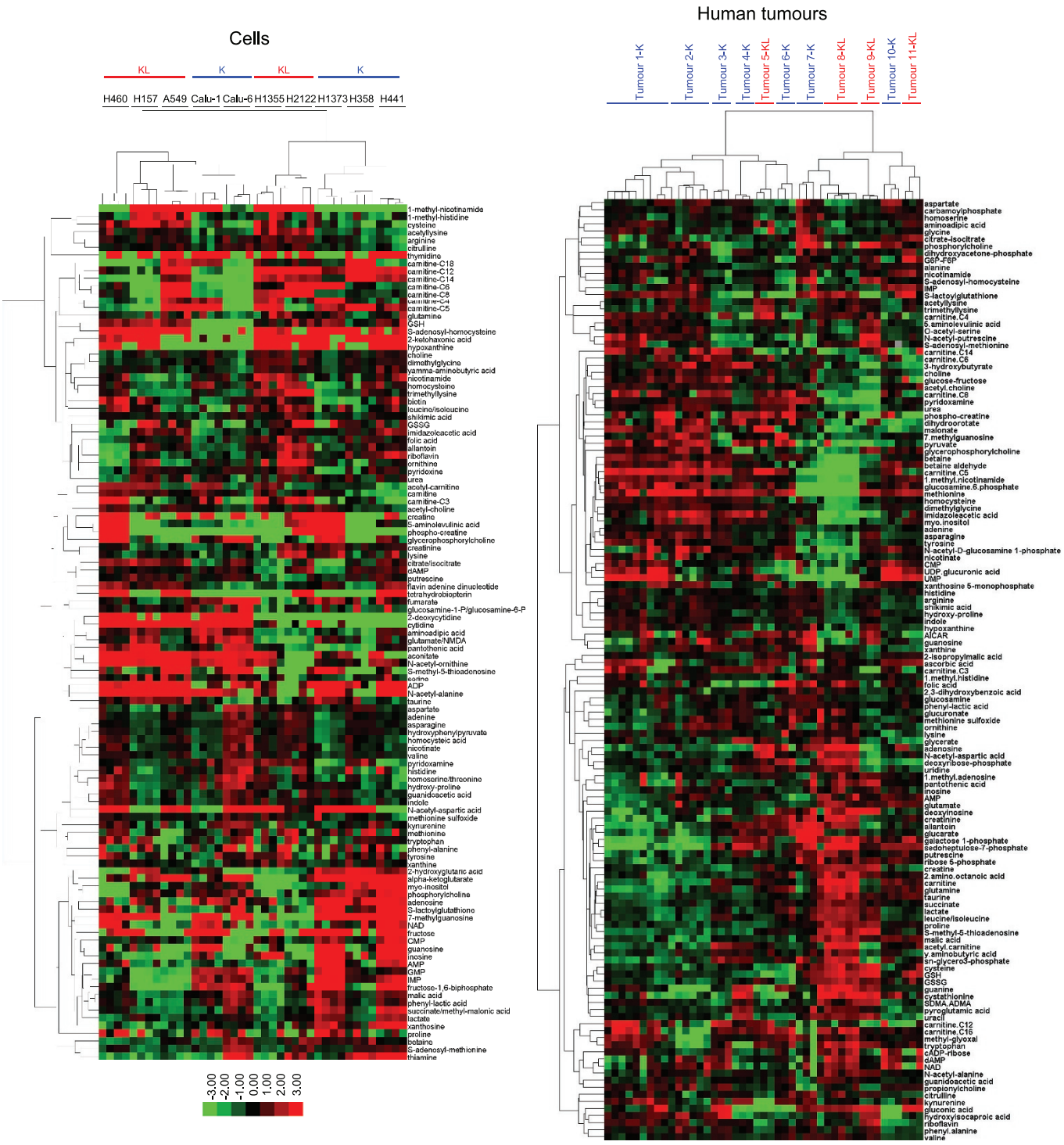

Extended Data Figure 2 | Metabolomic profiling of KL and K cancer cells and human NSCLC. Left, relative abundance of metabolites extracted from five KL (H157, A549, H460, H2122, H1355) and five K (Calu-1, Calu-6, H1373, H358, H441) cell lines. Peak areas of each metabolite were normalized by total ion count and the heat map displays the average value for each metabolite; $n = 4$ independent cultures for each cell line. Right, relative abundance of metabolites extracted from four KL human tumours (tumours 5-, 8-, 9- and 11-KL) and seven K human tumours (tumours 1-, 2-, 3-, 4-, 6-, 7- and 10-K). Peak areas of each metabolite were normalized by total ion count followed by mean normalization and the heat map displays the average value for each metabolite; $n = 3$ independent fragments for each tumour except tumour 2-K ($n = 6$), tumour 8-KL ($n = 6$) and tumour 1-K ($n = 9$). KL cell lines or tumours are indicated in red, K cell lines or tumours are indicated in blue. The colours in the heat map reflect a $\log_2$ scale.

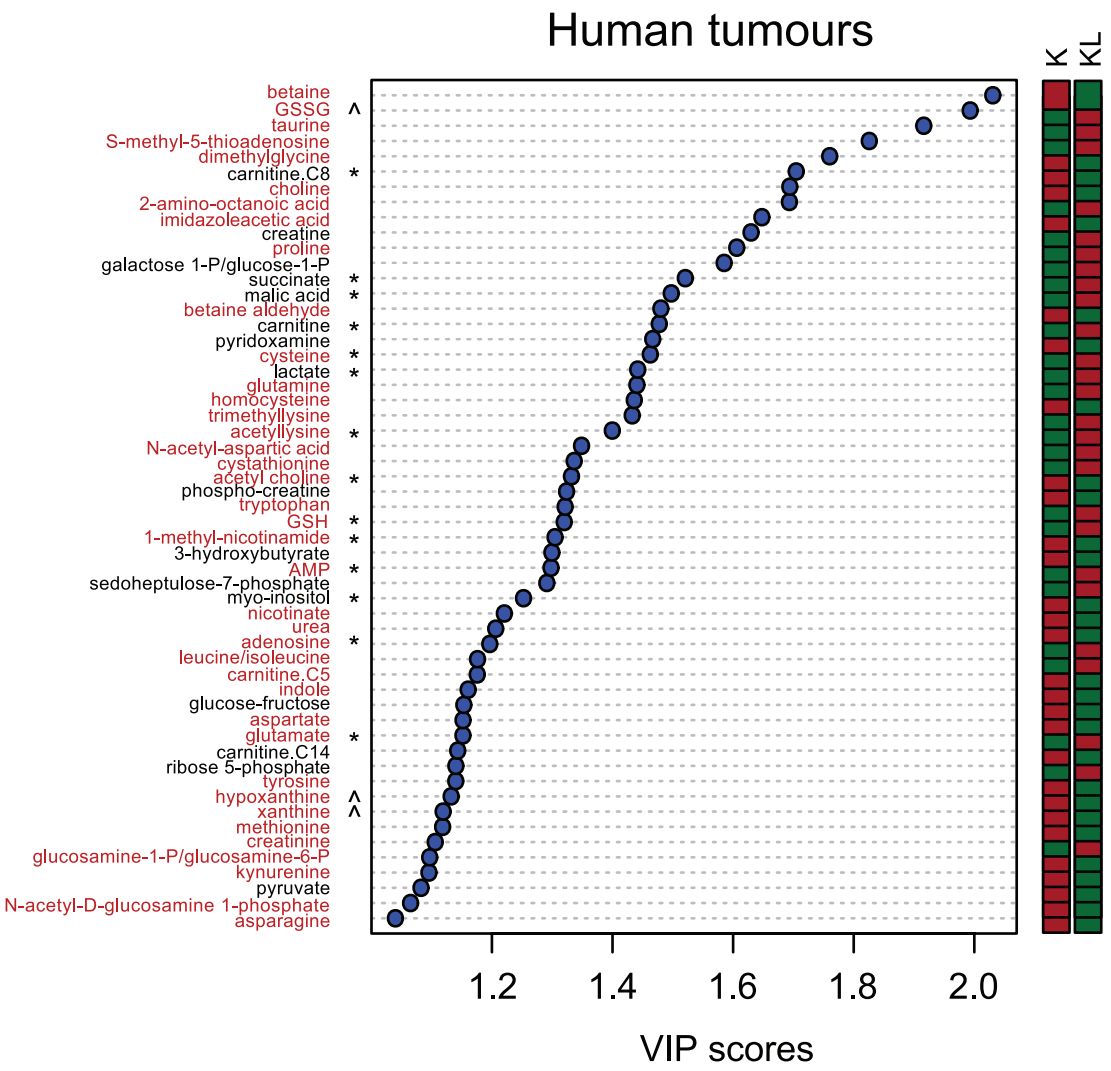

Extended Data Figure 3 | Metabolites differentiating between KL and K human NSCLC. Metabolites differentiating K from KL human tumours have variable importance in the projection (VIP) scores >1.0. Metabolites related to nitrogen metabolism are highlighted in red. The relative abundance of each metabolite is shown in the colour bar, where red indicates increased and green indicates decreased abundance. *Metabolites that also discriminated between K and KL cell lines in Fig. 1a and Supplementary Table 2. ^Metabolites closely related to those discriminating between K and KL cell lines in Fig. 1a (for example, hypoxanthine and xanthine in the tumours are related to xanthosine in the cell lines).

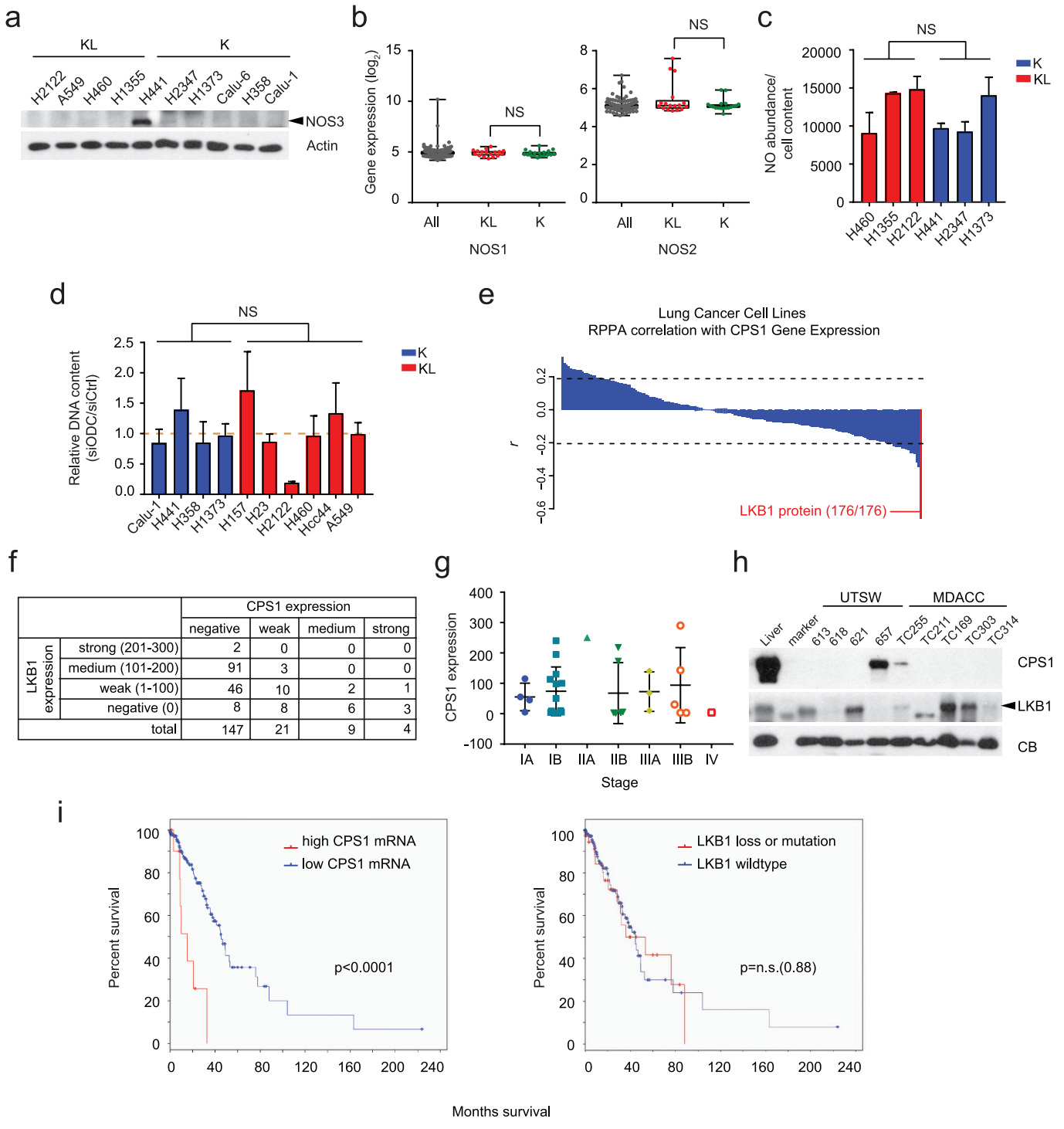

Extended Data Figure 4 | See next page for caption.

Extended Data Figure 4 | Nitrogen-related metabolic pathways in K and KL cells and inverse correlation between CPS1 and LKB1. a, Abundance of NOS3 protein in a number of K and KL cell lines. **b**, Distribution of mRNA abundance for *NOS1* and *NOS2* among 203 cell lines. Complete datasets including quantitative mRNA abundance of these genes are available in Supplementary Table 6. **c**, NOS activity in K and KL cells. Free NO was monitored in three cell lines of each genotype. Data are the mean ± s.d. of three independent cultures. **d**, Effect of silencing ornithine decarboxylase (ODC), an enzyme involved in polyamine synthesis from ornithine, in K and KL cells. Cell growth was measured by DNA content using a Perkin Elmer Victor X3 plate reader. Data are the mean ± s.d. of six independent cultures. **e**, Pearson's correlation coefficients (r) between *CPS1* mRNA and 176 proteins in 94 lung cancer cell lines. The rank of the LKB1 protein is indicated. Dashed lines demarcate correlation coefficients at a nominal $P = 0.05$. **f**, Scoring of LKB1 and CPS1 expression in TMA samples. For this analysis, tumours were considered positive if any CPS1 or LKB1 staining was detected (that is, an H-score greater than or equal to 1, as described in Methods); otherwise staining was considered negative. **g**, CPS1 protein expression in TMA tumour samples of different clinical stages. **h**, Abundance of CPS1 and LKB1 protein in patient-derived NSCLC xenografts. All patient-derived NSCLC xenografts had oncogenic KRAS mutations. **i**, Kaplan−Meier plot associating CPS1 expression with reduced survival. In the TCGA lung adenocarcinoma cohort (TCGA LUAD provisional, $n = 230$), LKB1 mutation or loss was observed in 19% of patient tumours ($n = 43$). For *CPS1*, a z-score threshold of 2.0 was used to identify tumours with high levels of expression; this included 5.2% ($n = 12$) of tumours. There was no difference in overall survival in patients with LKB1 alterations (deletion or mutation) versus those without an LKB1 alteration ($P = 0.88$). By contrast, patients whose tumours expressed high levels of *CPS1* mRNA had much shorter periods of overall survival compared to other patients (15.2 versus 45.3 months, $P < 0.0001$). The western blot and NOS activity assay were performed twice and the ODC silencing experiment was repeated three times or more. Statistical significance was assessed using a two-tailed Student's t-test. NS, not significant.

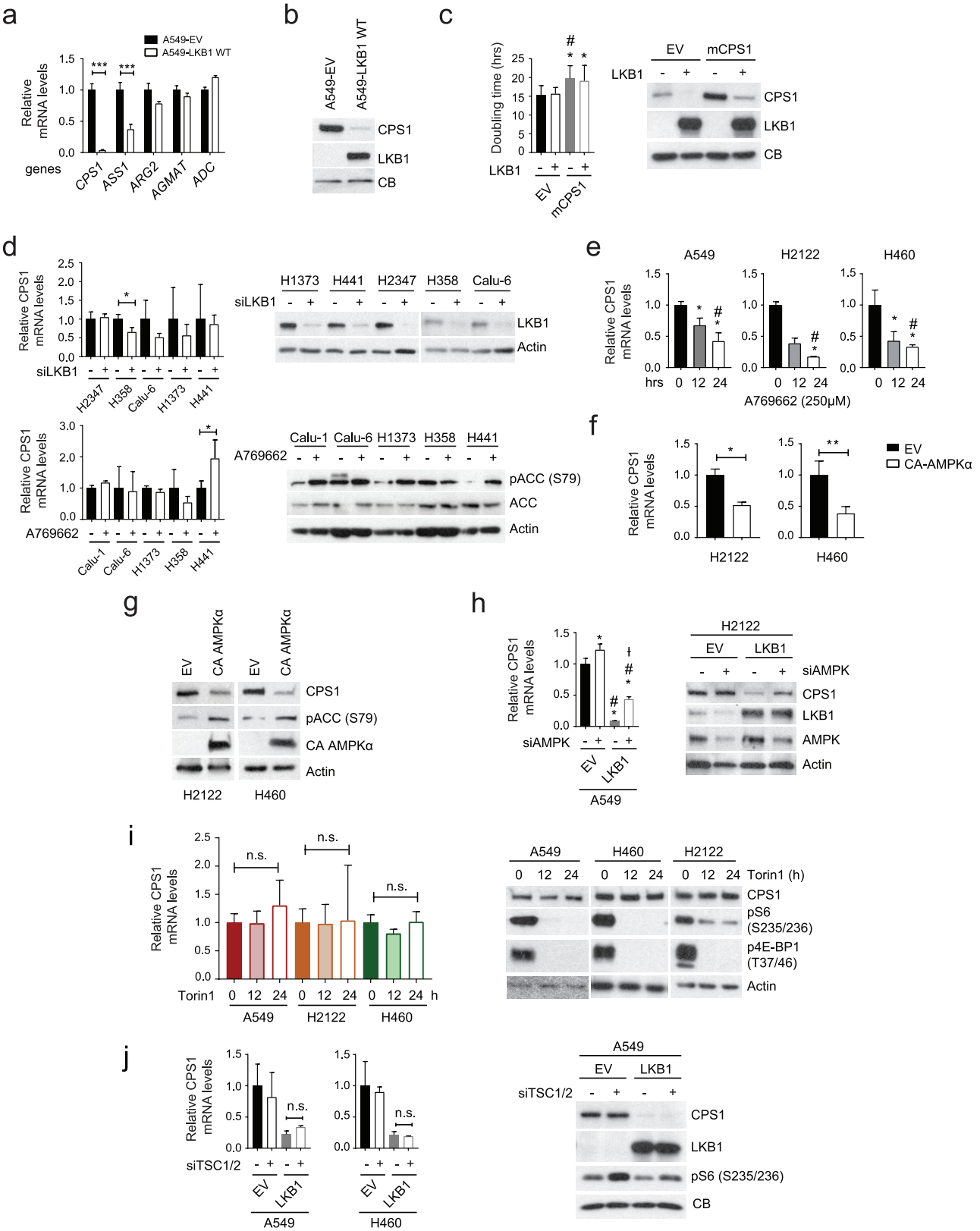

Extended Data Figure 5 | See next page for caption.

Extended Data Figure 5 | LKB1 suppresses CPS1 expression through AMPK. a, Expression of urea cycle and related enzymes in control A549 cells (empty vector, EV) and cells expressing wild-type LKB1. Data are the mean ± s.d. of three independent cultures. **b**, Abundance of CPS1 and LKB1 protein in A549 cells transfected with an empty vector (EV) or wild-type LKB1 (LKB1 WT). CB was used as a loading control. **c**, Left, the effect of expressing wild-type LKB1 or mouse CPS1 (mCPS1), alone or together, on H460 cell proliferation. EV is the empty vector control. Data are the mean ± s.d. of six or more independent cultures. Right, abundance of CPS1 and LKB1 protein in H460 cells stably expressing the empty vector or mCPS1. **d**, Top, effects of LKB1 silencing on *CPS1* mRNA expression in cells with oncogenic KRAS and wild-type LKB1 (K cells). Data are the mean ± s.d. of three or more independent cultures. Western blot shows the abundance of LKB1 protein in cells transfected with control siRNA or siRNA targeting *LKB1* (siLKB1). Bottom, effects of the AMPK activator A769662 on *CPS1* mRNA expression in K cells. Data are the mean ± s.d. of three or more independent cultures. Western blot shows the abundance of total and phosphorylated acetyl-CoA carboxylase (pAcc, S79) in cells treated with DMSO or A769662 (250 μM). **e**, Effects of A769662-mediated AMPK activation on *CPS1* mRNA expression in KL cells. Data are the mean ± s.d. of three or more independent cultures. **f**, Effects of constitutively active (CA) AMPK on *CPS1* mRNA expression in H2122 and H460 cells. Data are the mean ± s.d. of three or more independent cultures. **g**, Abundance of CPS1, pAcc and constitutively active AMPKα in H2122 and H460 cells transfected with an empty vector (EV) or constitutively active (CA) AMPKα. Actin was used as a loading control. **h**, Left, effects of AMPK silencing on *CPS1* mRNA expression in A549 cells without (EV) or expressing wild-type LKB1. Data are the mean ± s.d. of three independent cultures. Right, abundance of CPS1, LKB1 and AMPK proteins in A549 cells transfected with control siRNA or siRNA targeting *AMPK* (siAMPK). Actin was used as a loading control. **i**, Left, effects of the mTOR inhibitor Torin 1 on *CPS1* mRNA expression in KL cells. Data are the mean ± s.d. of four or more independent cultures. Right, abundance of CPS1, phosphorylated S6 (pS6) ribosomal protein and phosphorylated 4E-BP1 (p4E-BP1) in KL cells. Actin was used as a loading control. **j**, Left, effects of *TSC1* and *TSC2* (siTSC1/2) silencing on *CPS1* mRNA expression in A549 and H460 cells. Data are the mean ± s.d. of three independent cultures. Right, abundance of CPS1, LKB1 and pS6 in A549 cells. CB was used as a loading control. In **a**, **d**, **f**, **j**, statistical significance was assessed using two-tailed Student's *t*-tests. $*P < 0.05$, $**P < 0.01$, $***P < 0.001$, n.s., not significant. In **c**, **e**, **h**, **i**, statistical significance was assessed using a one-way ANOVA followed by Tukey's multiple comparisons test. In **c**, $*P < 0.05$ compared to EV and −LKB1; $\#P < 0.05$ compared to EV and +LKB1. In **e**, $*P < 0.05$ compared to no treatment; $\#P < 0.05$ compared to 12 h A769662 treatment. In **h**, $*P < 0.05$ compared to EV and control siRNA; $\#P < 0.05$ compared to EV and siAMPK; $\dagger P < 0.05$ compared to LKB1 and control siRNA. All experiments were repeated three times or more.

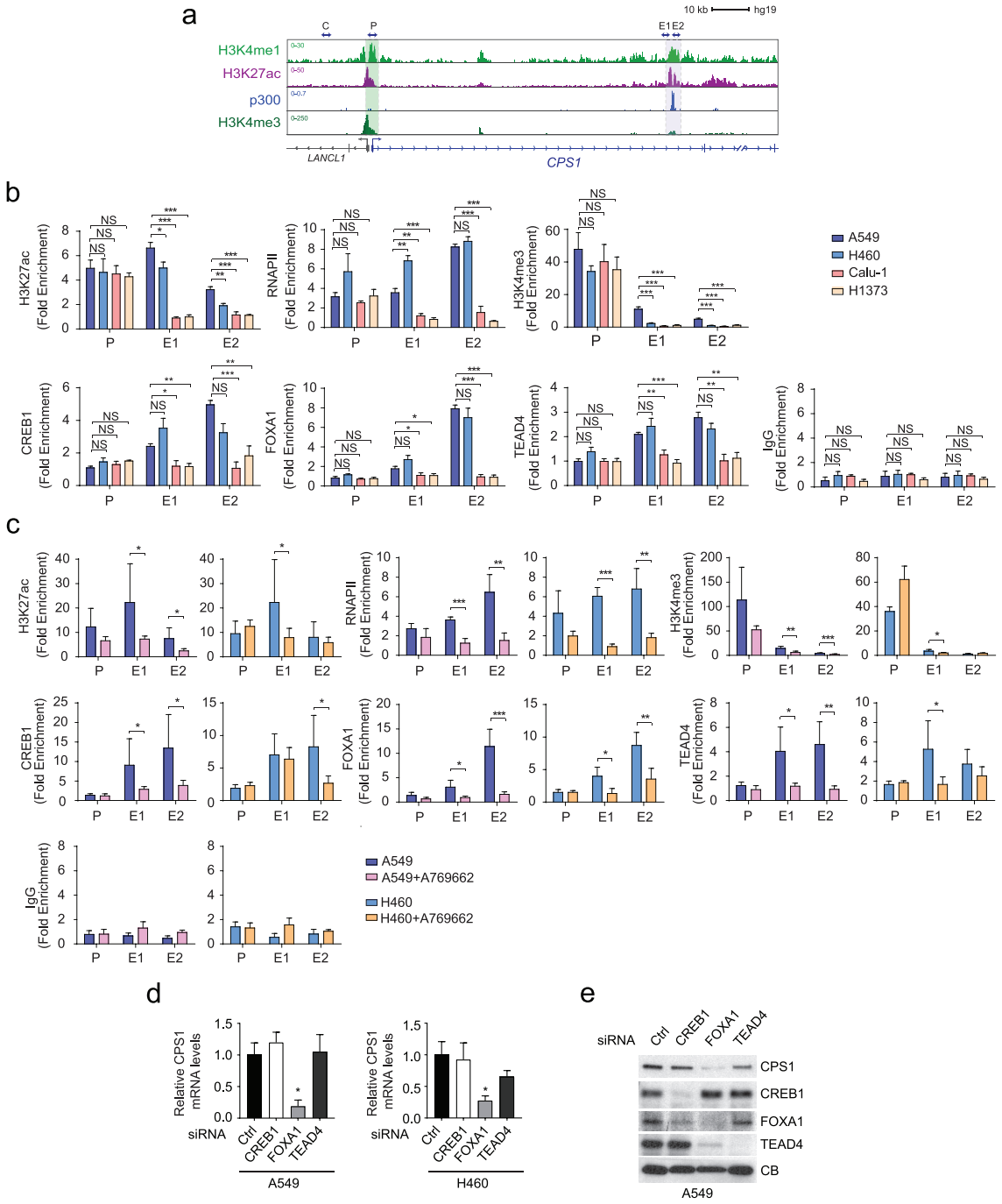

Extended Data Figure 6 | LKB1 regulates *CPS1* transcription through AMPK-mediated effects. a, Chromatin signatures at the *CPS1* locus in A549 cells. Promoter and enhancer sequences are shaded. Arrowheads indicate amplicons for control (C), promoter (P) and enhancer (E1, E2) regions for ChIP–qPCR in **b** and **c**. **b**, Chromatin occupancy of H3K27ac, RNAPII, H3K4me3, CREB1, FOXA1, TEAD4 and IgG (negative control) in KL (A549, H460) and in K (Calu-1, H1373) cells. Data are the mean ± s.d. of two independent cultures, each with two technical replicates (total $n = 4$). **c**, Chromatin occupancy of H3K27ac, RNAPII, H3K4me3, CREB1, FOXA1, TEAD4 and IgG in A549 and H460 cells treated with DMSO or 250 μM A769662. Data are the mean ± s.d. of three independent cultures, each with two technical replicates (total $n = 6$). **d**, Effects of *CREB1*, *FOXA1* and *TEAD4* silencing on *CPS1* mRNA expression in A549 and H460 cells. Data are the mean ± s.d. of three or more replicates. **e**, Abundance of CPS1, CREB1, FOXA1 and TEAD4 in A549 cells. CB was used as a loading control. In **b** and **c**, statistical significance was assessed using a two-tailed Student's *t*-test. $^*P < 0.05$, $^{**}P < 0.01$, $^{***}P < 0.001$, NS, not significant. In **d**, statistical significance was assessed using a one-way ANOVA followed by Tukey's multiple comparisons test. $^*P < 0.05$ compared to control. ChIP–qPCR in **b** was performed twice. All other experiments were repeated three times or more.

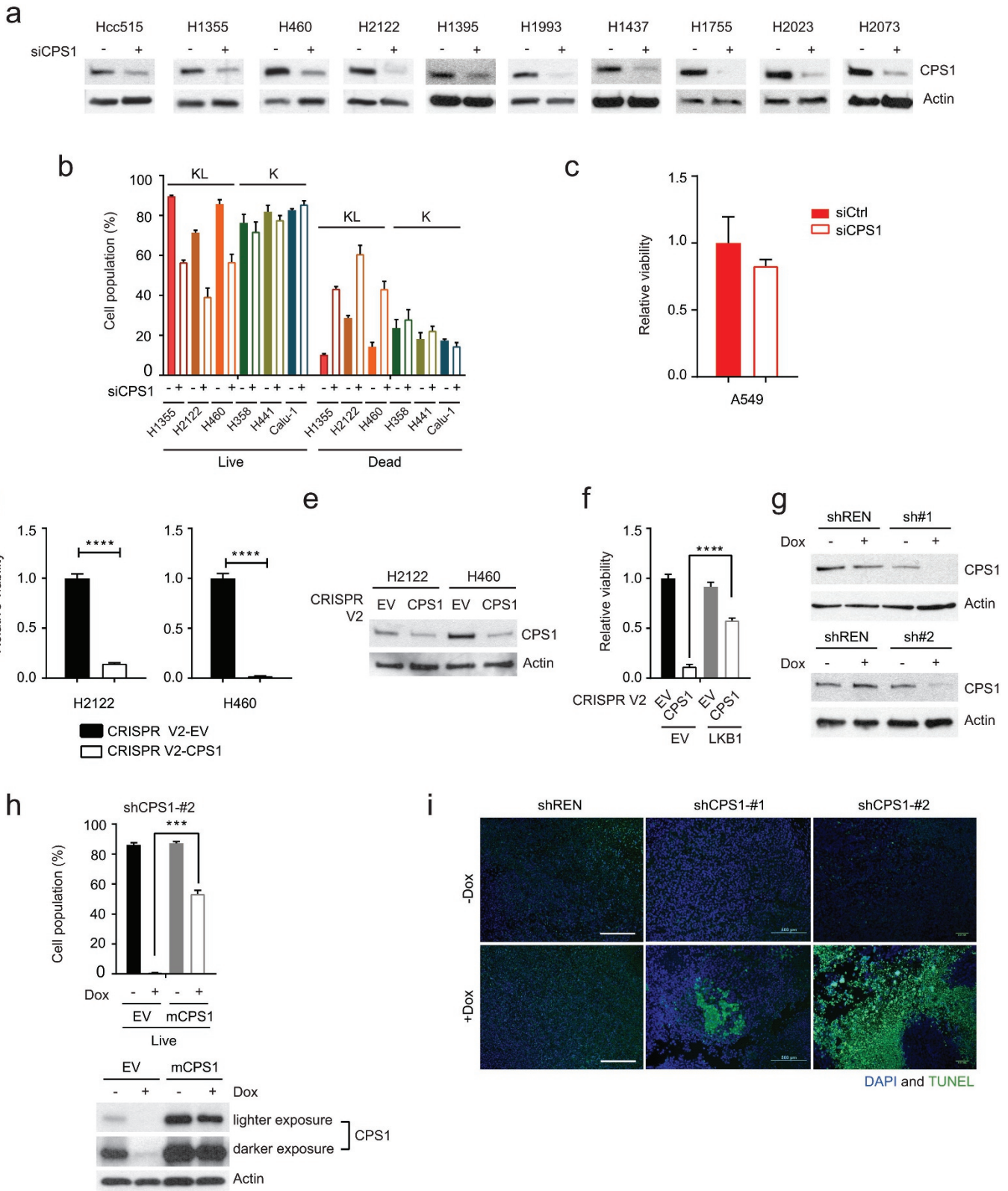

Extended Data Figure 7 | See next page for caption.

Extended Data Figure 7 | CPS1 addiction in a subset of NSCLC cell lines. a, Abundance of CPS1 protein in cell lines transfected with a control esiRNA or esiRNA directed against *CPS1*. **b**, Effect of *CPS1* silencing on cell death in K and KL cells. Data are the mean ± s.d. of three independent cultures. **c**, Effect of CPS1 silencing on A549 cell viability. Data are the mean ± s.d. of six independent cultures. **d**, Effect of lentiCRISPR–Cas9-mediated knockout of *CPS1* on viability in H2122 and H460 cells. CellTiter-Glo assays were performed on pools of *CPS1* knockout cells without first isolating clones. Data are the mean ± s.d. of six independent cultures. **e**, Abundance of CPS1 protein in H2122 and H460 control cells (EV) and a pool of cells infected with lentiviral CRISPR V2-CPS1 (CPS1). Actin was used as a loading control. **f**, Effect of knocking out *CPS1* on H460-EV and H460-LKB1-WT cells ($n = 6$). **g**, Abundance of CPS1 in H460 cells expressing shCPS1-1 (sh#1, top) and shCPS1-2 (sh#2, bottom) with or without Dox induction. shREN is a Dox-inducible control shRNA, and actin was used as a loading control. **h**, Top, effects of mouse CPS1 (mCPS1) expression on viability in H460 cells expressing shCPS1-2. Data are the mean ± s.d. of three independent cultures. Bottom, abundance of CPS1 protein in H460 cells expressing mCPS1 with or without shCPS1 induction. Actin was used as a loading control. **i**, TUNEL staining of tumour tissues. 4′,6-diamidino-2-phenylindole (DAPI) was used to stain DNA. Scale bars, 500 μm. In **d**, statistical significance was assessed using a two-tailed Student's *t*-test. ****$P < 0.0001$. In **f** and **h**, statistical significance was assessed using a one-way ANOVA followed by Tukey's multiple comparisons test. ***$P < 0.001$, ****$P < 0.0001$. Tissue TUNEL staining was performed once. Viability assay (**f**) was performed twice. All other experiments were repeated three times or more.

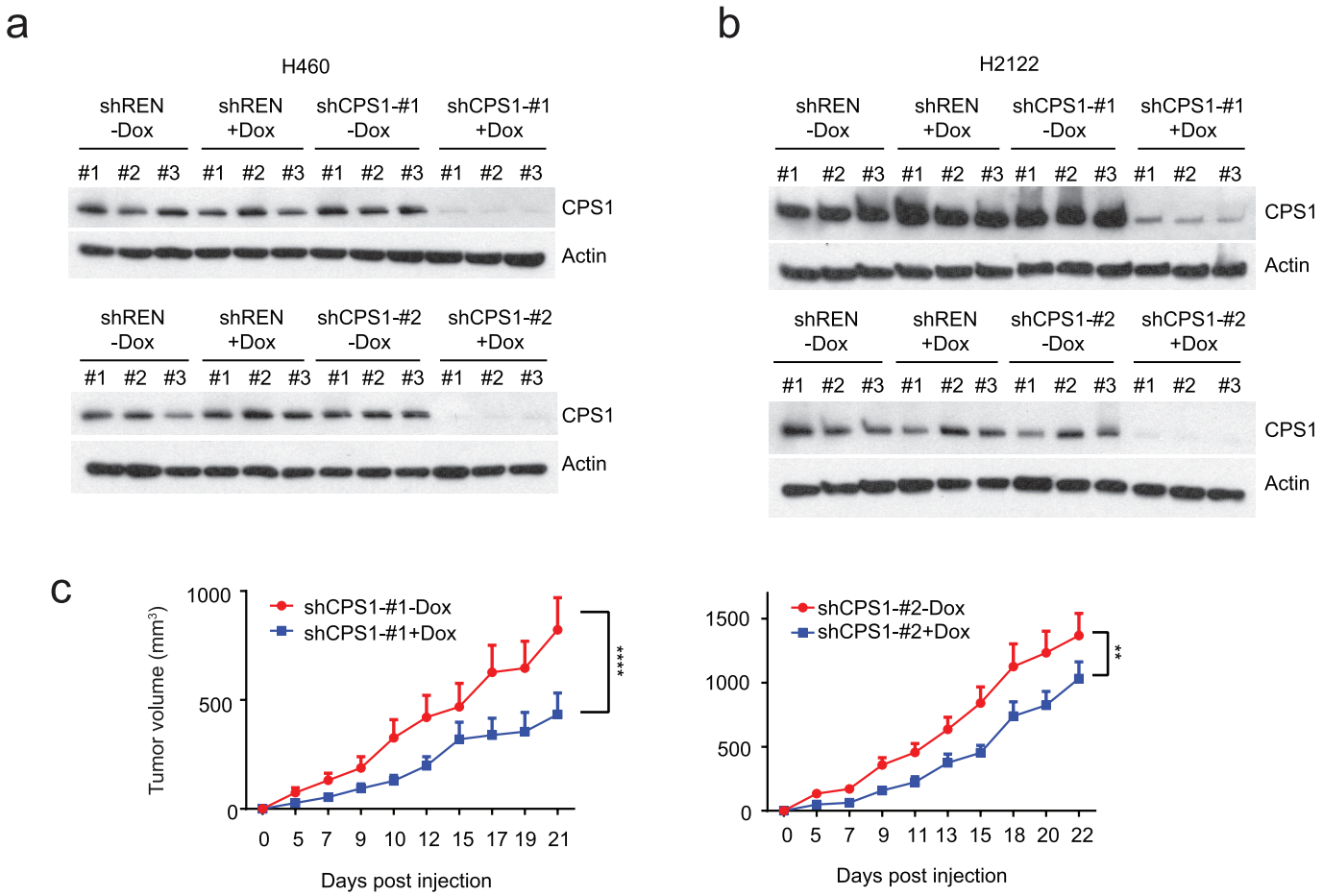

Extended Data Figure 8 | CPS1 expression and xenograft growth. **a**, **b**, Abundance of CPS1 protein in H460 (**a**) and H2122 (**b**) xenografts expressing shCPS1-1 (top) and shCPS1-2 (bottom) with or without Dox induction. shREN is a Dox-inducible control shRNA and actin is a loading control. **c**, Effect of Dox-induction of shCPS1-1 (left) and shCPS1-2 (right) on H2122 xenograft growth. Nude mice were injected subcutaneously with H2122 shCPS1 (shCPS1-1, shCPS1-2) cells and Dox (200 mg kg^{-1}) was introduced one day later. Each group ($n = 8$) is presented as mean tumour volume ± s.e.m. Statistical significance was assessed using a two-way ANOVA. $^{**}P < 0.01$, $^{****}P < 0.0001$. Experiments were performed once ($n = 8$ mice).

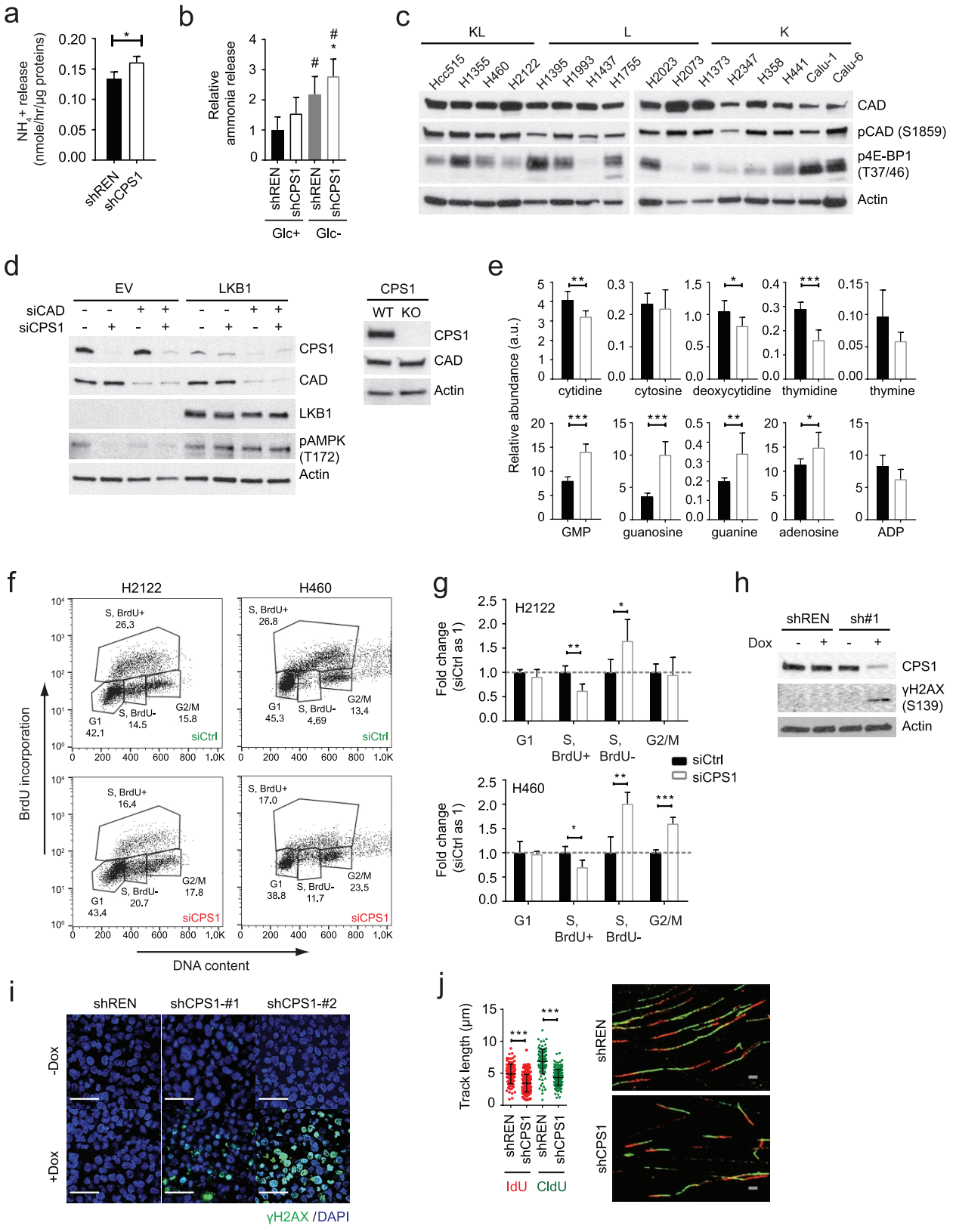

Extended Data Figure 9 | See next page for caption.

Extended Data Figure 9 | *CPS1* silencing results in pyrimidine depletion and DNA damage. a, Ammonia release from H460 cells expressing shREN or shCPS1-1 ($n = 3$). **b**, Ammonia release from H460 cells expressing shREN or shCPS1-2 in the presence and absence of glucose (Glc). Glucose deprivation provides a positive control for enhanced ammonia release in cancer cells (see 'Metabolic Assays' in the Methods). Data are the mean ± s.d. of three independent cultures, each with three technical replicates (total $n = 9$). **c**, Abundance of total CAD, phosphorylated CAD (pCAD) and phosphorylated 4E-BP1 (p4E-BP1) in K, L and KL cells. Actin was used as a loading control. **d**, Left, CPS1, CAD, LKB1 and phosphorylated AMPK (pAMPK) abundance in H460 cells without (EV) or with LKB1 expression. Cells were transfected with siRNA targeting *CAD* or *CPS1*. Actin was used as a loading control. Right, abundance of CPS1 and CAD protein in wild-type or CPS1-knockout H460 cells. Actin was used as a loading control. **e**, Relative abundance of pyrimidines and purines during expression of shREN (closed bars) or shCPS1-1 (open bars) ($n = 6$). **f**, Effects of CPS1 silencing on BrdU incorporation ($n \geq 3$). DNA content and BrdU incorporation were assessed by flow cytometry following dual staining with BrdU and propidium iodide. **g**, Effect of CPS1 silencing on cell cycle distribution ($n = 4$). **h**, Abundance of CPS1 protein and γH2AX in H460-shREN and -shCPS1-1 cells with or without Dox induction. **i**, γH2AX in H460 xenografts. DAPI was used to stain DNA. Scale bars, 40 μm. **j**, Effects of CPS1 silencing on DNA track length measured by iododeoxyuridine (IdU) and chlorodeoxyuridine (CldU) incorporation. At least 104 tracks were measured for each condition. Scale bars, 2 μm. In **b**, statistical significance was assessed using a one-way ANOVA followed by Tukey's multiple comparisons test. $^{*}P < 0.05$ compared to shREN with glucose; $^{\#}P < 0.05$ compared to shCPS1 with glucose (Glc). In **a**, **e**, **g**, **j**, statistical significance was assessed using a two-tailed Student's *t*-test. $^{*}P < 0.05$, $^{**}P < 0.01$, $^{***}P < 0.001$. Tissue staining was performed once. Nucleotide measurements and DNA fibre assays were performed twice. All other experiments were repeated three times or more.

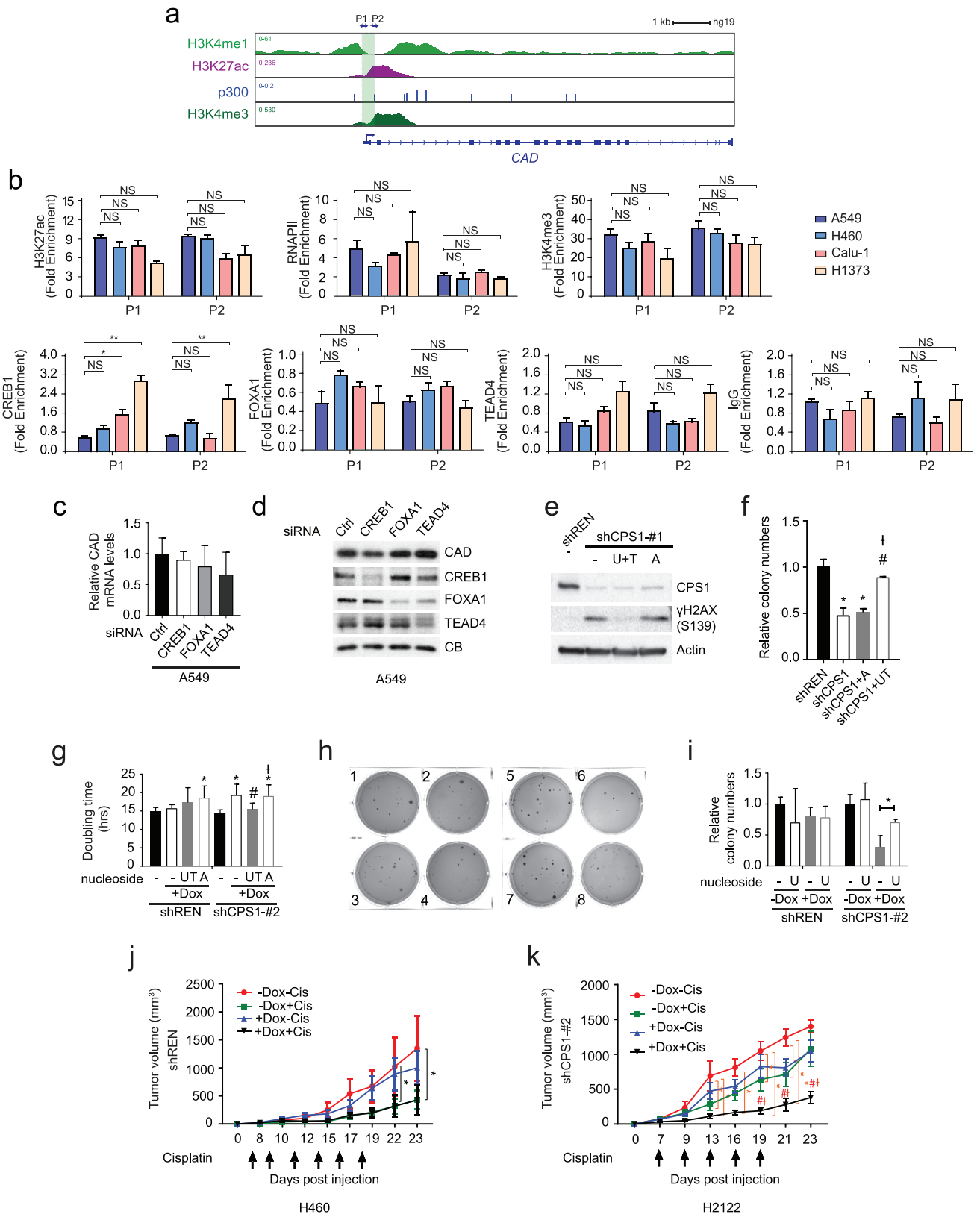

Extended Data Figure 10 | See next page for caption.

Extended Data Figure 10 | Regulation of *CAD* transcription is distinct from that of *CPS1* and pyrimidine nucleosides rescue DNA damage and proliferation of *CPS1* silenced cells. a, Chromatin signatures at the *CAD* locus in A549 cells. Promoter sequences are shaded. Arrowheads indicate amplicons for promoter (P1, P2) regions for ChIP–qPCR in **b**. **b**, Chromatin occupancy of H3K27ac, RNAPII, FOXA1, H3K4me3, CREB1, TEAD4 and IgG (negative control) in KL (A549, H460) and in K (Calu-1, H1373) cells. Data are the mean ± s.d. of two independent cultures, each with two technical replicates (total $n = 4$). **c**, Effects of *CREB1*, *FOXA1* and *TEAD4* silencing on *CAD* mRNA expression in A549 cells. Data are the mean ± s.d. of three independent cultures, each with two technical replicates (total $n = 6$). **d**, Effects of CREB1, FOXA1 and TEAD4 silencing on CAD protein abundance in A549 cells. CB was used as a loading control. **e**, The effect of supplementing culture medium with uridine and thymidine (UT) or adenosine (A) (100 μM final concentration) on γH2AX abundance in Dox-induced H460 cells expressing shREN or shCPS1-1. **f**, The effect of supplementing culture medium with uridine and thymidine or adenosine on anchorage-independent colony formation of H460 cells expressing shCPS1-1 ($n = 3$). The time point is after 20 days of Dox induction. **g**, Effects of nucleoside supplementation on proliferation of H460 cells expressing shCPS1-2. Data are the mean ± s.d. of three independent cultures, each with three technical replicates (total $n = 9$). **h**, Colonies from Fig. 4f. 1–4: shREN, 5–8: shCPS1-2; 1, 5, no treatment; 2, 6, Dox treatment; 3, 7, Dox and uridine and thymidine; 4, 8, Dox and adenosine. **i**, The effect of supplementing with uridine alone on anchorage-independent colony formation of H460 cells expressing shCPS1-2. Data are the mean ± s.d. of three independent cultures. **j**, Growth of subcutaneous H460 shREN-derived xenografts in presence and absence of Dox, with or without cisplatin. Mean tumour volume ± s.e.m. are shown for each group ($n = 4$) **k**, Growth of subcutaneous H2122 shCPS1-#2-derived xenografts in nude mice in the presence and absence of Dox (200 mg kg^{-1}) introduced one day after implantation with or without cisplatin treatment (intraperitoneal injection at 2 mg kg^{-1} for 5–6 doses). Mean tumour volume ± s.e.m. are shown for each group ($n = 4$). In **b**, **i**, statistical significance was assessed using a two-tailed Student's *t*-test. $*P < 0.05$, $**P < 0.01$, NS, not significant. In **f**, **g**, statistical significance was assessed using a one-way ANOVA followed by Tukey's multiple comparisons test. In **j**, **k**, statistical significance was assessed using a two-way ANOVA followed by Tukey's multiple comparisons test. In **f**, $*P < 0.05$ compared to shREN; $\#P < 0.05$ compared to shCPS1; $\dagger P < 0.05$ compared to shCPS1 and adenosine. In **g**, first four bars: $*P < 0.05$ compared to shREN without Dox; second four bars: $*P < 0.05$ compared to shCPS1 without Dox; $\#P < 0.05$ compared to shCPS1 with Dox; $\dagger P < 0.05$ compared to shCPS1 with Dox and uridine and thymidine. In **j**, **k**, $*P < 0.05$ compared to −Dox and −Cis; $\#P < 0.05$ compared to −Dox and +Cis; $\dagger P < 0.05$ compared to +Dox and −Cis. Xenograft experiments were performed once, ChIP–qPCR was performed twice and all other experiments were performed three times or more.

CORRECTION

https://doi.org/10.1038/s41586-019-1133-3

Author Correction: CPS1 maintains pyrimidine pools and DNA synthesis in KRAS/LKB1–mutant lung cancer cells

Jiyeon Kim, Zeping Hu, Ling Cai, Kailong Li, Eunhee Choi, Brandon Faubert, Divya Bezwada, Jaime Rodriguez-Canales, Pamela Villalobos, Yu-Fen Lin, Min Ni, Kenneth E. Huffman, Luc Girard, Lauren A. Byers, Keziban Unsal-Kacmaz, Christopher G. Peña, John V. Heymach, Els Wauters, Johan Vansteenkiste, Diego H. Castrillon, Benjamin P. C. Chen, Ignacio Wistuba, Diether Lambrechts, Jian Xu, John D. Minna & Ralph J. DeBerardinis

Correction to: *Nature* https://doi.org/10.1038/nature22359, published online 24 May 2017.

In this Letter, we used a multiple reaction monitoring (MRM) liquid chromatography–tandem mass spectrometry (LC–MS/MS) method to estimate relative quantities of carbamoyl phosphate in non-small-cell lung cancer (NSCLC) cell lines (Extended Data Fig. 1c). Further analysis has revealed that the MRM transition of 140/79 detects phosphorylethanolamine as well as carbamoyl phosphate. We improved the selectivity of the method by using more specific but less sensitive transitions (142/44 for phosphorylethanolamine and 140/97 for carbamoyl phosphate), and confirmed that the reported signal in Extended Data Fig. 1c was phosphorylethanolamine, not carbamoyl phosphate. The method using these new transitions did not reproducibly detect carbamoyl phosphate, even in freshly prepared samples. To overcome the lability of carbamoyl phosphate in acidic conditions and increased temperatures[1,2], we developed a derivatization method to transform it to a more stable 2-(2-pyridinyl)-hydrazinecarboxamide after a nucleophilic addition from 2-pyridylhydrazine. Although this method detects the intended derivative from a pure carbamoyl phosphate standard, the abundance of this product in NSCLC cell lines was below the background level. The low-level background of this derivatized product probably appeared through the slow, spontaneous conversion of 2-pyridylhydrazine to 2-(2-pyridinyl)-hydrazinecarboxamide under some conditions (for example, 2-pyridylhydrazine may react with cyanate ion at ambient temperature; see the formation of compound 66 in ref. [3]). We estimate the threshold for the detection of carbamoyl phosphate to be approximately 10 nanomoles, and we conclude that carbamoyl phosphate in our NSCLC extracts is below this threshold. We emphasize that these new data do not detract from the major findings of the paper: that LKB1 suppresses CPS1 expression in NSCLC, and that NSCLCs with concurrent mutations in KRAS and LKB1 require CPS1 to maintain pyrimidine pools. The original Letter has not been corrected online.

1. Lowenstein, J. M. & Cohen, P. P. Studies on the biosynthesis of carbamylaspartic acid. *J. Biol. Chem.* **220**, 57–70 (1956).
2. Wang, Q., Xia, J., Guallar, V., Krilov, G. & Kantrowitz, E. R. Mechanism of thermal decomposition of carbamoyl phosphate and its stabilization by aspartate and ornithine transcarbamoylases. *Proc. Natl Acad. Sci. USA* **105**, 16918–16923 (2008).
3. Haviv, F. et al. 3-[1-(2-Benzoxazolyl)hydrazino]propanenitrile derivatives: inhibitors of immune complex induced inflammation. *J. Med. Chem.* **31**, 1719–1728 (1988).